2012

Finite-Difference Time-Domain Modeling of Nickel Nanorods

Joseph Steele Parris
Virginia Commonwealth University

Finite-Difference Time-Domain Modeling of Nickel Nanorods

A thesis submitted in partial fulfillment of the requirements for the degree of Master of Science in Physics / Applied Physics at Virginia Commonwealth University.

By

J. Steele Parris

B.S. in Physics

Minor in Astronomy

Hampden-Sydney College, 2009

M.S. in Physics/Applied Physics

Virginia Commonwealth University, 2012

Major Director:

Dexian Ye, Ph.D., Assistant Professor, Department of Physics

Virginia Commonwealth University

Richmond, Virginia, 23284

1 May 2012

Acknowledgments

I would first and foremost like to thank Steven Johnson and J.D. Joannopolous for developing Meep as an open-source software package that can be used freely, as well as maintaining the Meep Mail Archives as a friendly and open method to share help amongst users.

I also want to thank my friends and family for their support throughout the last few years. I would also like to thank the graduate students of the VCU Physics department, especially Mathias Auer, Louis Franzel, Sean Kenney, and Chuck Wingfield. If it weren't for you all, I would probably go into teaching high school to later on owning an RV.

I also would like to thank the faculty and staff members of the VCU Department of Physics for their support and help. Special thanks go to Drs. Baski and Reshchekov for their worthwhile input and critique of my research and presentation skills. Lastly, I'd like to thank my advisor, Dr. Dexian Ye, for his invaluable time and effort in aiding me with research and writing, as well as preparing me for the "great beyond."

I dedicate this work to my wife, Sabrina. Everything I've done here in Virginia I did for you.

Table of Contents

Table of Figures

Abstract

FINITE-DIFFERENCE TIME-DOMAIN MODELING OF NICKEL NANORODS

By Joseph Steele Parris

A thesis submitted in partial fulfillment of the requirements for the degree of Master of Science at Virginia Commonwealth University.

Virginia Commonwealth Univerity, 2012

Major Director: Dexian Ye, Ph.D., Assistant Professor, Department of Physics

Theoretical and experimental plasmonics is a growing field as a method to create near fields at sub-wavelength distances. In this thesis, a finite-difference time-domain method is used to simulate electromagnetic waves onto a thin film that present of nickel nanorods with sharp apexes. The absorbed, transmitted, and reflected fields were shown to depend linearly on silver film thickness and nanotip length. The electric field is visualized along the tip to show strong charge density along the base of the tip's apex and how that density changes for wavelength, metal, and source tilt. Lastly, the study shows gold film on the nanotip apex provides the largest enhancement of the electric field for the wavelengths 532, 572, and 633 nm.

1. Introduction

1.1 Motivation

Recent years have seen a boom in surface plasmon research, both experimentally[1] and theoretically[2]. The concept of plasma oscillations in conductive media has been around for quite some time, utilizing this phenomenon has been of a recent occurrence[3]. Surface plasmon experiments have been seen in many fields from physics[4] to antibody-antigen detection in health sciences[5]. Explaining surface plasmons theoretically has been a popular contemporary topic due to faster computer processors and more powerful computational techniques, allowing researchers to model charge density waves in a number of different scenarios[6]. This project consists of the latter of the two: a theoretical study of nickel nanorods through a finite-difference time-domain analysis of electromagnetic waves to understand the optical properties of the thin film on the nanotips. Combining the surface plasmon resonance of silver and gold with atomically sharp tips allows strong fields to form on the nanoscale, with applications ranging from nanophotonics[7], photovoltaics[8], to even biosensing[9]. This section will discuss the physics behind the simulations, the production, and the applications of these nickel nanorods.

1.2 Electromagnetic Waves

This thesis describes the interaction of electromagnetic waves with nanostructures. We begin by noting that electromagnetic waves follow from Maxwell's equations[10]:

$$\nabla \cdot \vec{E} = \rho / \varepsilon_o \qquad \nabla \times \vec{E} = -\frac{\partial \vec{B}}{\partial t} \qquad (1.1)$$

$$\nabla \cdot \vec{H} = 0 \qquad \nabla \times \vec{H} = \vec{J} + \frac{\partial \vec{E}}{\partial t}$$

Here, $\vec{E}$ represents the electric field, ρ is the volume charge density, $\vec{H}$ is the magnetic field, and $\vec{J}$ is the current density. Combining these equations together in free space (ρ=0, $\vec{J}$=0) leads to

$$\nabla^2 \vec{E} = \frac{1}{c^2}\frac{\partial^2 \vec{E}}{\partial t^2} \quad \text{and} \quad \nabla^2 \vec{B} = \frac{1}{c^2}\frac{\partial^2 \vec{B}}{\partial t^2}. \qquad (1.2)$$

These equations are the classical wave equations, which suggests that the electric field and magnetic field oscillate in unison. The form of the electric wave would be

$$\vec{E} = \mathrm{Re}\{\vec{E}_o e^{i\omega t}\} \qquad (1.3)$$

which is a plane wave. This is the type of wave we'll be using as the electromagnetic source for the simulations.

It is important to note that the nanostructures involved in this project are smaller than the wavelengths of light being simulated. Despite the difference of sizes, not only do Maxwell's equations apply and are still valid on the nanoscale, but the equations are used to solve systems such as of photonic crystals to calculate the blocking of certain frequencies transmitting through the crystal[11].

1.3 Plasmons

The electromagnetic wave is incident onto a metallic structure leading to some motion with "free electrons" contained in the metal. This motion leads to a "volume plasmon", a charge density wave that oscillates internally. The dielectric constant of the metal is given by the equation

$$\varepsilon_p(\omega) = 1 - \frac{\omega_p^2}{\omega^2}, \tag{1.4}$$

where ε_p is the permittivity of the metal, ω is the frequency of the electromagnetic wave, and ω_p is the classical plasma frequency (in cgs units) defined as

$$\omega_p = \sqrt{\frac{4\pi n e^2}{m_e}}, \tag{1.5}$$

where n is the electron concentration, e is the fundamental charge of the electron, and m_e is the mass of the electron. Table 1 shows some metals that will be used in these simulations and their respective plasma energies.

Metal	$\hbar\omega_p$ (eV)
Ag	9.01
Au	9.03
Cu	10.83
Ni	15.92

Table 1: Metals and their plasma energy. [Ref 12]

When the frequency of the electromagnetic wave is more than the plasma frequency, the permittivity is positive—the wave propagates through the material. On the other hand, when the light frequency is less than the plasma frequency, the permittivity becomes negative—the light is reflected from the bulk metal. This explains why visible and infrared light are reflected off most metals while ultraviolet and higher frequency electromagnetic waves pass through metals.

The oscillation of the electrons in the bulk is useful to explain the reflectivity of metal, but the oscillations on the metal-dielectric interface yields interesting properties. When excitation waves are incident on a metal-dielectric interface, there is a change in frequency of the plasmon wave [13]. This effect is known as a surface plasmon, and the change of frequency (ω_{sp}) is dictated by the following equation[14]

$$\omega_{sp}{}^2 = \frac{\omega_p{}^2}{(1+\varepsilon)} \quad , \qquad (1.6)$$

where ε is the permittivity of the dielectric. Since the dielectric is usually air, the dielectric constant is approximately 1 and so the ω_p:ω_{sp} ratio is 1: $\sqrt{2}$. This downward shift of the surface plasmon frequency allows a few metals to have plasmonic resonances within the visible spectrum—gold, silver and copper are the usual candidates. Even so, this charge excitation occurs in the geometry of the metal, such as thin films, nanoparticles, and distances between nanoparticles[13].

Two variations of surface plasmons can exist. The first is the surface plasmon polariton which is a charge density wave that travels along the surface via waveguide[2]. The other, which is the subject matter for this project, is the localized surface plasmon[15]. These are charge density oscillations that are confined to a metallic object such as nanoparticles, and generally the dimensions of these objects will play a large part in determining the surface plasmon resonance.

1.4 Nickel Nanorod Fabrication

The design of the dielectric model in the simulations is based off of nanorods fabricated by Ye *et al.* through the method of oblique angle deposition[16]. Nickel is deposited on a silicon (100) substrate at room temperature using the oblique angle deposition technique while the substrate is

rotating—this yields a large population of nickel nanorods that have sharp apexes. When the nickel rods are formed, a 30 nm layer of silver film is deposited normally onto the tips of the nickel nanorods. The silver will be the container of the localized surface plasmons, since the surface plasmon resonance for silver is within the visible spectrum.

The combination of localized surface plasmon resonance and atomically sharp tips produce very strong electric fields around the apex of the rods. This has an advantage with any application that requires strong electric fields yet limited space.

The shape of the tip used in the simulation will mimic that of these fabricated nickel nanotips. The scanning electron microscope image in Figure 1 show (a) the top and (b) side view of the nickel nanotips fabricated by Ye *et al.* as well as (c) the top and (d) side view of the same tips with a 30 nm layer of silver deposited on the tops of the tips. These images show that the apex is not conical but rather has a pyramidal form, as the inset in (a) displays. This is largely due to the crystalline nature of nickel which happens to be face-centered cubic.

1.5 Applications

The strong field localizations produced by the surface plasmons are very useful in smaller devices that operate from electric fields. For instance, solar cells require the strong electric fields in a p-n junction that would create hole-electron pairs[17]. Second generation solar cells are thin films of p-type and n-type semiconductors; they reduce cost and weight as compared to first generation cells which are composed of p-type and n-type monocrystalline silicon junctions[18]. Because the amount of active layer is reduced, however, the likelihood of hole-electron pair is reduced and thus lower efficiency.

To increase the efficiency of these second generation solar cells, a layer of metal nanoparticles can be sandwiched between the thin films, especially if there are multiple p-n

junction layers (effective for absorbing multiple wavelengths of light)[19]. As light propagates through the solar cell's layers, nanoparticles that are of a specific size and spacing will absorb the light and yield surface plasmons. These surface plasmons will develop intense electric fields which will, in turn, increase the production of electron-hole pairs at the p-n junction[20,21].

Another application of metallic nanoparticles is for Raman scattering[22]. This phenomenon occurs when you shine a single wavelength of light onto a molecule it forces the bonds of the molecule to start oscillating into a harmonic motion. The energy not consumed into the vibrational mode will inelastically scatter out as a different wavelength. Measuring the spectrum of this scattered light yields a fingerprint analysis of the molecule. The issue, however, is if one wants to test a sample that is highly diluted; since the intensity of the spectrum depends on the number of molecules vibrating at the same frequency, the essential peaks will be drowned out by noise[23].

A modified method, known as surface-enhanced Raman spectroscopy (SERS), has been developed that allows smaller concentrations of samples to be detected[24]. The essential difference is that the sample is placed on a "rough" metal surface. This coarse metal surface amplifies the number of Raman scattered photons from the detecting molecules. One of the current theories is that light incident onto a roughened metal surface excites surface plasmons, thus creating localized, strongly oscillating electric fields. When the detecting molecule exists in this field, the likelihood of vibrating and emitting a Raman scattered photon increases.

Chapter 1 Figures

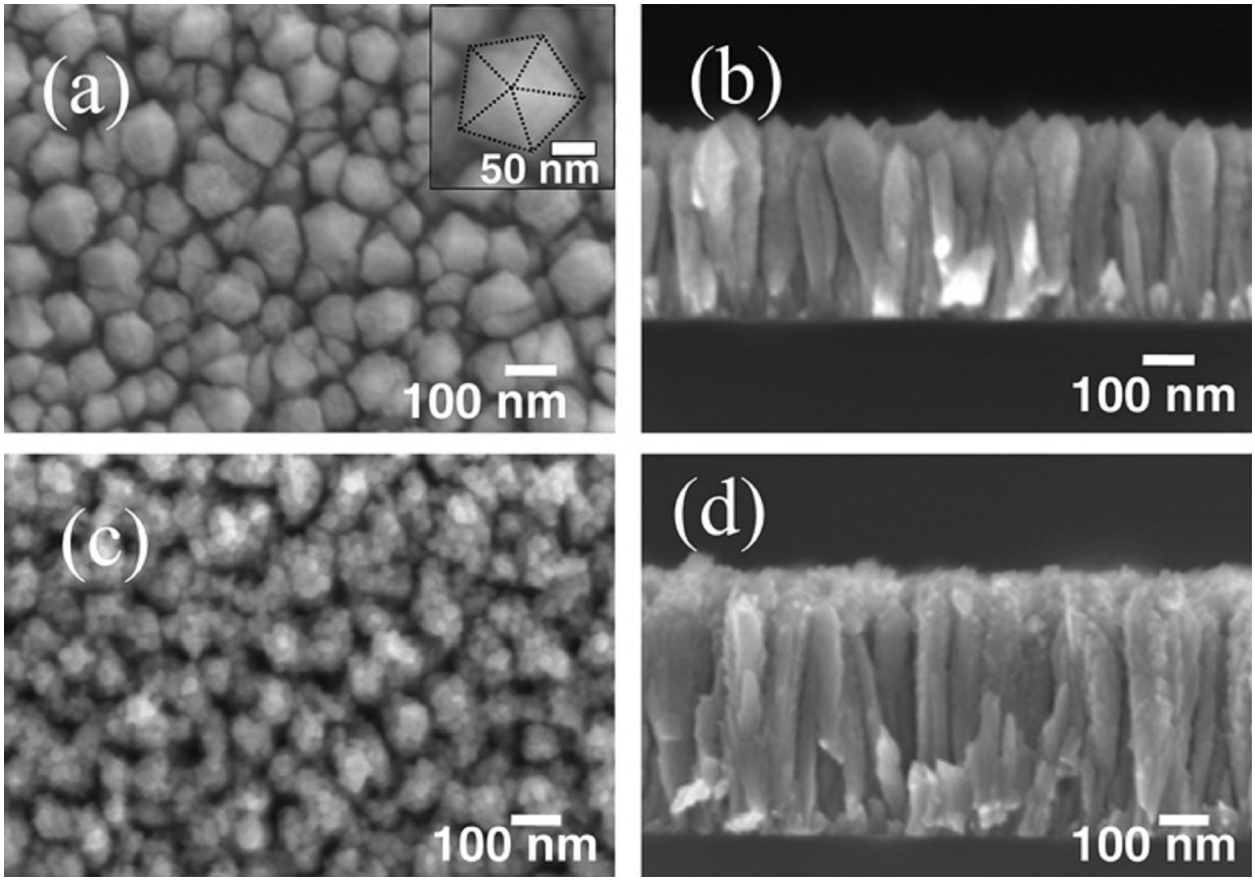

Figure 1: Fabricated Ni nanotips top view (a), and side view (b) via scanning electron microscopy (SEM). Also, said Ni nanotips with a 30nm silver film deposited on the surface, top view (c) and side view (d).[Ref. 16]

2. The Finite-Difference Time-Domain Method

2.1 Theory of FDTD Method

The method of simulation modeling to be used is known as the finite-difference time-domain (FDTD) method[25]. Ampere's and Faraday's Law in free space, respectively,

$$\frac{\partial \vec{E}}{\partial t} = \frac{1}{\varepsilon_o} \nabla \times \vec{H} \tag{2.1}$$

$$\frac{\partial \vec{H}}{\partial t} = -\frac{1}{\mu_o} \nabla \times E \tag{2.2}$$

show that the electric field and the perpendicular magnetic field are dependent on each other. If the curl equations for one dimension is solved so that the electromagnetic wave is propagating in the z-axis, the electric field is oscillating in the x-axis, and the magnetic field is oscillating in the y-axis.

$$\frac{\partial E_x}{\partial t} = -\frac{1}{\varepsilon_0} \frac{\partial H_y}{\partial x} \tag{2.3}$$

$$\frac{\partial H_y}{\partial t} = -\frac{1}{\mu_0} \frac{\partial E_x}{\partial x} \tag{2.4}$$

To simplify these differential equations, the finite difference method is applied to the derivatives, as seen below[26]:

$$\frac{E_x^{n+1/2}(k)-E_x^{n-1/2}(k)}{\Delta t}=-\frac{1}{\varepsilon_0}\frac{H_y^n(k+1/2)-H_y^n(k-1/2)}{\Delta x} \tag{2.5}$$

$$\frac{H_y^{n+1}(k+1/2)-H_y^n(k+1/2)}{\Delta t}=-\frac{1}{\mu_0}\frac{E_x^{n+1/2}(k+1)-E_x^{n+1/2}(k)}{\Delta x} \tag{2.6}$$

Here, *n* refers to the proper time frame and *k* refers to the proper spatial position. To find out the specific time, it is $t = n\cdot\Delta t$; likewise, to find the specific location, it is $z = k\cdot\Delta x$. Note two things with these approximations, the first being the electric and magnetic fields are "leapfrogging" by 1/2 increments, and the second fields depend either on information from the past and the future or on information from neighboring cells[27]. Solving these equations with respect to the field in the future forms the following:

$$E_x^{n+1/2}(k)=E_x^{n-1/2}(k)-\frac{\Delta t}{\varepsilon_0\cdot\Delta x}[H_y^n(k+1/2)-H_y^n(k-1/2)] \tag{2.7}$$

$$H_y^{n+1}(k+1/2)=H_y^n(k+1/2)-\frac{\Delta t}{\mu_0\cdot\Delta x}[E_x^{n+1/2}(k+1)-E_x^{n+1/2}(k)] \tag{2.8}$$

One of the key features of the FDTD method is that it breaks the dielectric model into discrete blocks. Each block is noted as a *Yee cell*, where each electric field vector is surrounded by magnetic field vectors that are a half-block distance away, and likewise for the magnetic fields[25]. Figure 2 gives a visual explanation of how the Yee cell works, showing that the electric fields and magnetic fields are perpendicular to each other yet are half of a cell distance apart from each other. Changing the permittivity and permeability constants to mimic optical behavior seen in real materials will develop better models of how electromagnetic waves propagate through said material.

Another key feature of FDTD is the use of a step process to solve for Maxwell's equations[28]. Initially, it will start one time step by solving only the electric field across the space. The magnetic fields of all space will be solved in the next time step, and the process is repeated. When the equations are solved in three dimensions, a three-dimensional dielectric geometry of the construct can be designed in order to simulate a real construct of similar appearance. Boundary conditions must be developed as well. For instance, once the electromagnetic wave impinges the wall of the cell that contains the dielectric, the wave has the following options: reflect back, become absorbed, or transmit through to the opposite wall (to create a periodic boundary). On certain parts of the cell, the wave should not reflect or transmit through the wall—otherwise the wave would impinge the dielectric twice which is what is not observed in a real-time experiment. To prevent reflecting waves, generally a parameter called perfectly matched layer (PML) will be applied to absorb the wave if it impinges the boundary[29].

There are other methods to solve Maxwell's equations—finite element analysis is one such method[30]. FDTD, however, is useful due to its ability to program the optical properties of metals through the Drude-Lorentz model as well as its speed given that its rigid geometry allows only basic shapes.

2.2 Meep

The computational electromagnetic method used in the modeling is Meep (version 1.1.1). It was built by MIT as an open-source program under the GNU General Public License[27]. Meep uses a programming language called Scheme, which is a variation of Lisp. While initially set up for the use of studying electromagnetic waves in photonic crystal structures, Meep is a great program to

deal with dispersive mediums such as metals. The model that Meep uses to create dispersive media is the Lorentz-Drude model which gives the form[12]

$$\varepsilon(\omega) = \varepsilon_f(\omega) + \varepsilon_b(\omega), \tag{2.9}$$

where $\varepsilon_f(\omega)$ is the permittivity from free electron effects (intraband effects) in the system, based from the Drude model, and $\varepsilon_b(\omega)$ is the permittivity from the bound electron effects (interband effects) in the system, based from the Lorentz's contribution. More specifically, each component is described as:

$$\varepsilon_f(\omega) = 1 - \frac{f_o \omega_p^2}{\omega(\omega - i\Gamma_o)}, \tag{2.10}$$

$$\varepsilon_b(\omega) = \sum_{j=1}^{k} \frac{f_j \omega_p^2}{(\omega_j^2 - \omega^2) + i\omega\Gamma_j}, \tag{2.11}$$

where ω_p is the plasma frequency, k is the number of oscillators with frequency ω_j, f_j represents the strength of said oscillators, and $1/\Gamma_j$ is the lifetime of each oscillator. The graphs in Figure 3 show the Lorentz-Drude model, simulated through Meep, with both real and imaginary parts of three metals' dielectric function (silver, gold, nickel) which is dependent on frequency. These functions are comparable to both theoretical and experimental functions found in Raçik *et al.*[12]. The real part of the dielectric is negative as to keep both functions on the same quadrant of the graph.

The three metals that will be modeled in our simulations will be nickel for the majority, as well as silver and gold for the thin apex layer. The constants that will be used for these metals had to be scaled for our unit length discussed below, and they are available in the appendix.

2.3 Dielectric Setup

Another interesting feature of Meep is that it is dimensionless[28]. The program uses its length units based on how a dielectric geometry is set. For instance, if a test dielectric is 1 μm long, Meep sets a unit length in the program as 1 which, in real world application, equals 1 μm. This, in turn, will affect the wavelength of the light source--if it is desired to have a source of near-infrared light (say, 2 μm), the excitation source wavelength can be calculated to be 2 units long. Another aspect of this is that the speed of light is dimensionless as well, and it is set as c = 1, which means the light in the simulation propagates 1 unit length every 1 unit of time.

In our simulation, the unit length is established at 100 nm. The cell which will contain the dielectric material is 1600 nm by 200 nm by 200 nm. The nickel rod starts off with a 400 nm by 100 nm by 100 nm block centered in the cell, with the longer axis parallel to the x-axis. The top of the nickel block is carved at 45° slopes to be established as the "apex". The thickness of the metal film that will coat the apex (gold or silver) will be 30 nm. In addition, the block lies erect on top of a 100 nm nickel coating and a thick silicon substrate ($\varepsilon = 12$). The schematic of the model is found in Figure 4 as both the side view and top-down view. These dimensions will be the ones used consistently through the simulations unless otherwise noted.

The PML for these simulations will be placed a far distance above the tip as well as deep within the silicon substrate. For these simulations, the PML thickness was set at 1 unit directly along the x-direction cell walls. The electromagnetic wave sources will be determined based on the type of information desired. For the light localization and enhancement studies, the source will be fixed at a particular wavelength. For the reflection-transmission-absorption studies, the source will emit a wide wavelength. The details of the sources will be brought up per study.

Chapter 2 Figures

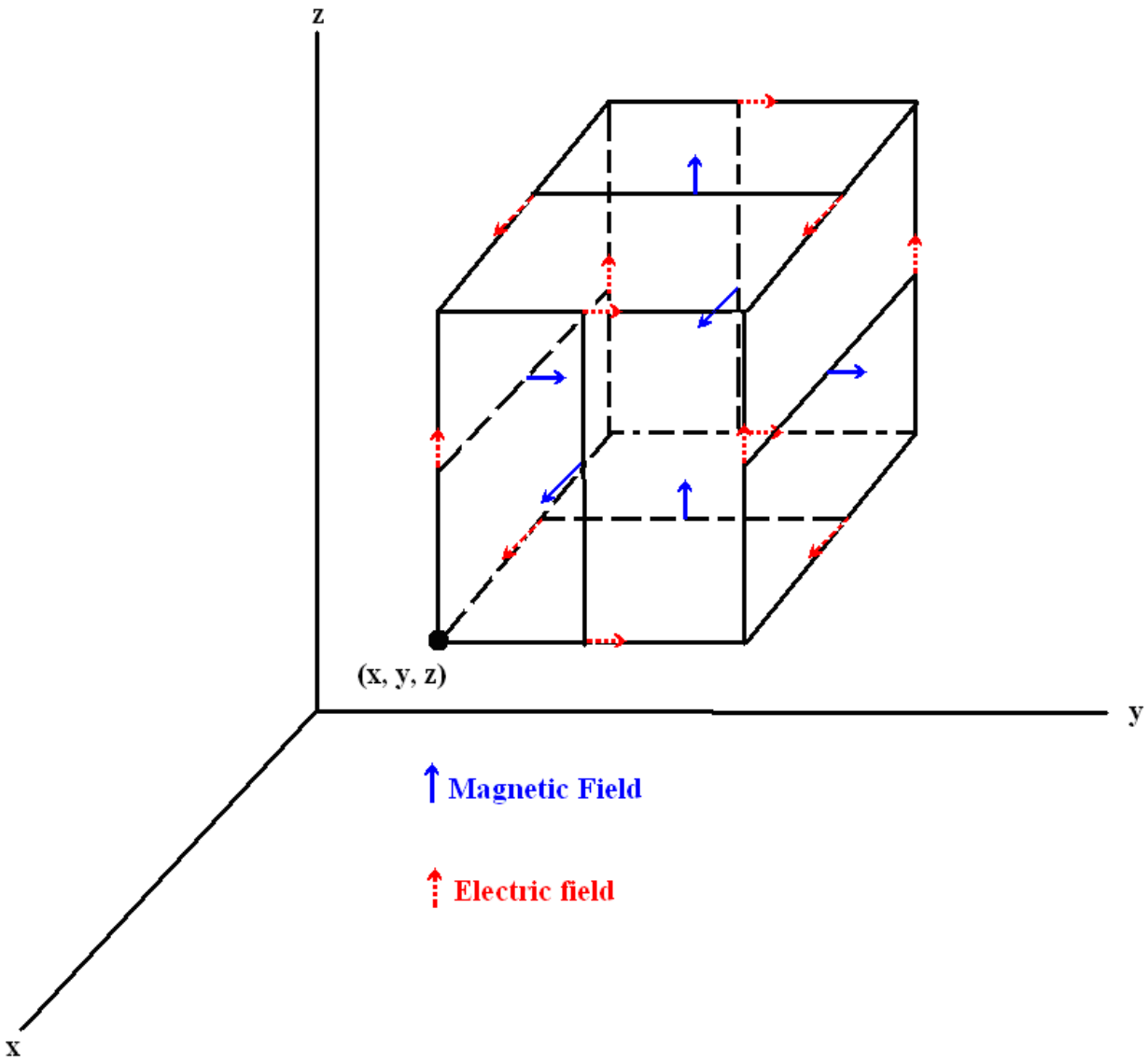

Figure 2: Yee Cell used in FDTD method (adapted from Ref 25).

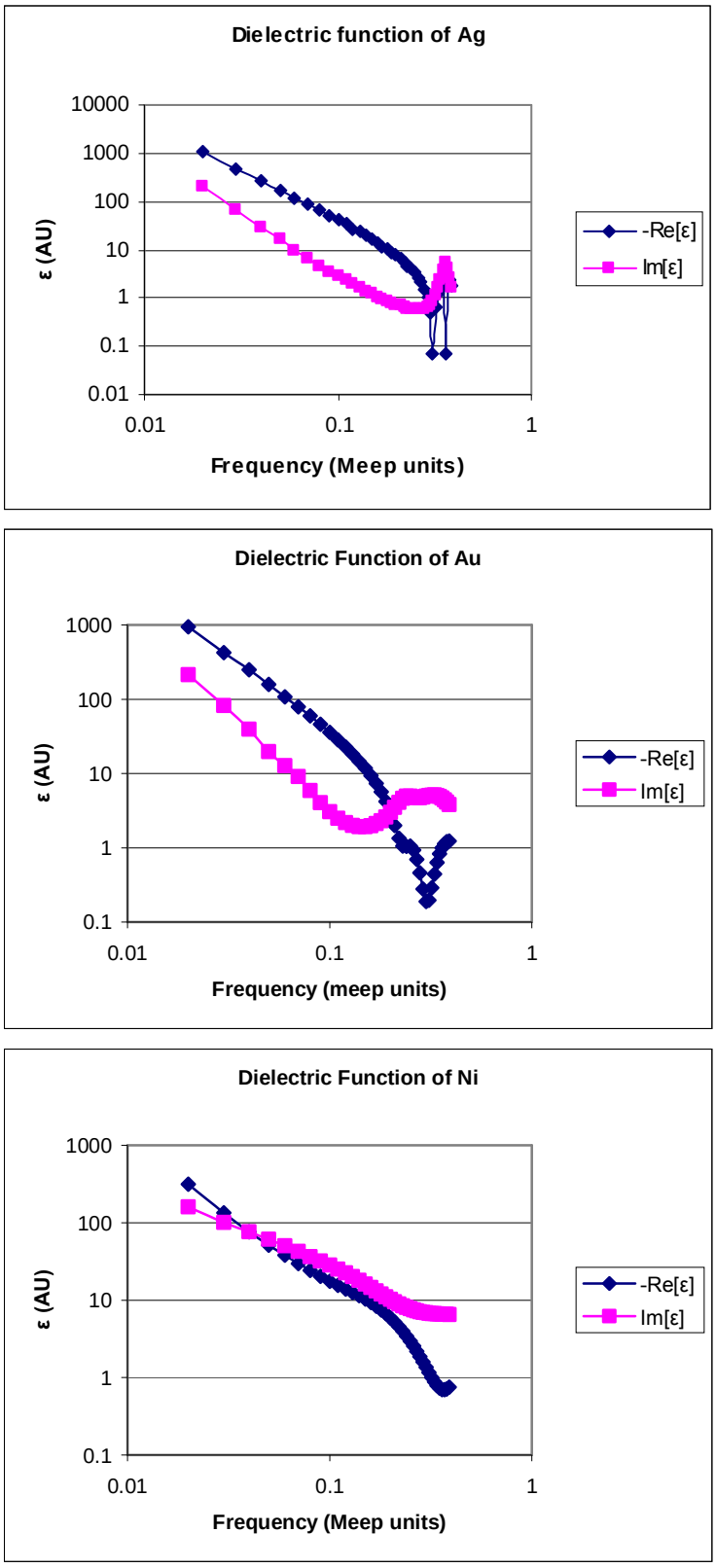

Figure 3: The Lorentz-Drude model the metal's (real and imaginary) dielectric function through Meep for silver, gold, and nickel.

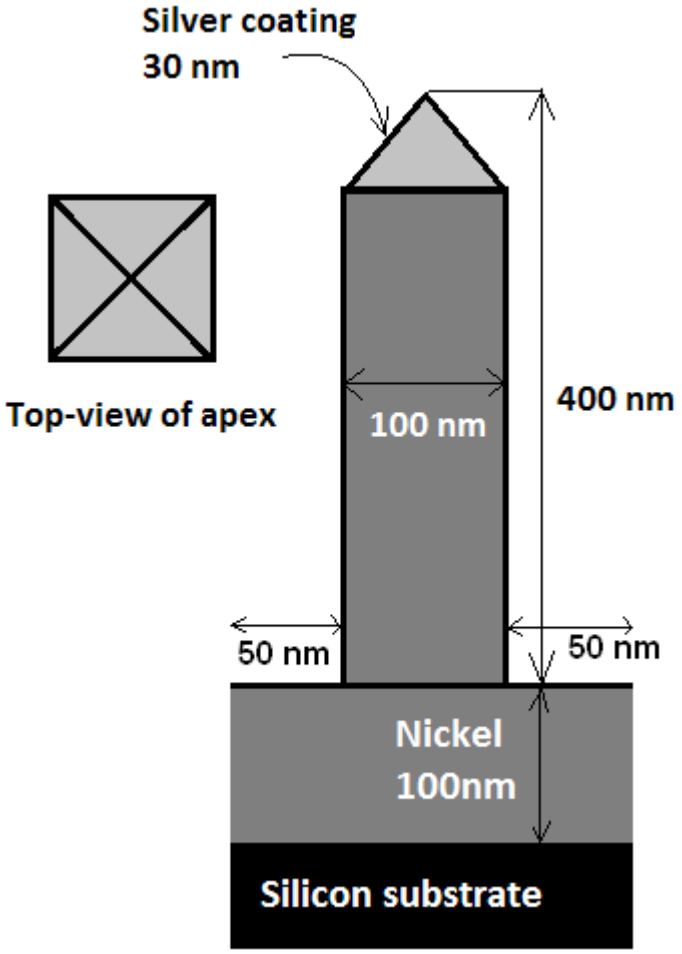

Figure 4. Diagram of the simulated nickel nanorod with silver tip.

3. Absorption, Transmission, & Reflection Spectra

3.1 Absorption, Transmission, and Reflection

Measuring the absorption, reflection, and transmission as a function of photon energy has its roots in experimental methods such as UV-VIS and IR spectroscopies. In these methods, a wide spectrum of light is passed through a substance, where a monochromatic detector is set up on the opposing side. The transmitted light is compared to the source of the light, for which it shows the percentage of light that passes through the substance. This spectrum, known as the transmission spectra, depends on the thickness (length of the optical path) of the substance, as well as its attenuation factor.[31] The attenuation factor is the amount of light that did not pass through the substance and into the detector (the absorption spectra). Generally, it is given in the form of the Lambert-Beers law,

$$I = I_o e^{-\alpha z}. \qquad (3.1)$$

Here, I is the intensity of transmitted light, I_o is the intensity of the source, z is the depth for which the light penetrates the material, and α is the attenuation factor.

As for reflection, generally the percentage of light that is reflected from an interface at normal incidence is determined by this equation

$$R = \left(\frac{n_1 - n_2}{n_1 + n_2} \right)^2 \qquad (3.2)$$

where n_1 and n_2 are the indices of refraction of each boundary. Of course, if the material happens to have an index of refraction that is dependent on the frequency of light, there is much more to consider. In our case, there exists a conductive medium, so that when light impinges on the surface, part of the electric field is lost to electron oscillation as discussed above [32].

The main purpose of calculating the reflectance, absorbance, and transmittance is to attempt to create models based off of the dimensions of the nickel nanotip to create an optimized substrate for SERS. A maximized absorbance is desired since it shows the largest transfer of energy between the excitation wave and the surface plasmons on the tip, which requires a minimized reflectance and transmittance.

3.2 Simulation Procedure

The simulation for our metallic thin film will use the consistent form that was observed through the SEM images.[16] In order to pass a spectrum of light through the thin film, Meep's Gaussian pulse source was used which the electric field is roughly proportional to

$$\vec{E} \propto \exp\left[-i\omega t - \frac{(t-t_o)^2}{w^2}\right] \qquad (3.3)$$

where $\vec{E}$ is the electric field of the source, ω is the frequency of the source, w is the temporal width of our Gaussian pulse, t is the current time, and t_o is the initial time of the source. This source emits electromagnetic waves of a wide spectrum of frequencies which the detectors will be able to interpret the strength of each frequency.

There will be two "detectors" or planes that, as the wave passes through it, will determine the strength of the electric field as a function of frequency. One detector will be placed in the silicon substrate some small distance away from the nickel base film which will detect the electric field that passes through the metal (transmission detector). The second detector will be

placed above the metal film which will detect the electric field that is reflected back towards the source (reflection detector).

Power in Meep is defined as the integral of the cross products of the electric field and magnetic field over the flux area.

$$P(\omega) = \mathrm{Re}\left[\hat{n} \cdot \int \vec{E}_{\omega}^{\,*}(\vec{x}) \times \vec{H}_{\omega}(\vec{x}) d^2\vec{x}\right] \tag{3.4}$$

To calculate the transmittance, the simulation was run without any material (free space) in order to measure P_{source}, and then it ran with the film in order to measure $P_{dielectric}$; the transmittance is the ratio of the fields

$$T = \frac{P_{dielectric}}{P_{source}} \tag{3.5}$$

Calculating the reflectance is more complicated because the detector counts both the field from the source as well as the reflected field[27]. The simulation has to be run twice, once with the film in order to measure P_{source} and once without the film in order to measure $P_{dielectric}$. As the next simulation gathers information on the field, it will subtract the field from before (when it was just the source), then compare it to the field of the source so that

$$R = \frac{P_{dielectric} - P_{source}}{P_{source}}. \tag{3.6}$$

The absorbance A, which is the light that is neither transmitted nor reflected, is calculated by

$$A = 1 - T - R \tag{3.7}$$

The spectral range was set between 550 nm and 715 nm.

3.3 Absorption-Transmission-Reflection Spectra

Figure 5 shows the absorption, transmission, and reflection spectra simulated through Meep for the dimensions outlined in Chapter 2. After running the simulations for different modifications to the geometry of the nanotip, several repeating features were noticed in the spectra. These features were a minimum in the reflectance as well as maxima for the transmittance and absorbance. In order to compare the different modifications, these optimal wavelengths were plotted against the following changes in geometry: nanorod width, nanorod length, silver apex thickness, and nickel film thickness.

3.3.1 Nanorod Width

The optimal wavelengths for absorbance, transmittance, and reflection as a function of tip width are charted in Figure 6. In this figure, increasing the width of the nickel nanotip from 80 to 130 nm shows an exponential increase of the maximum wavelength of transmittance yet a decrease in transmittance from 65% to 20%. Both the minimum reflection and maximum absorption wavelengths seem to peak at 680 and 660 nm, respectively. While the reflectance drops to approximately 0.12% near 120 nm width, the absorbance increase from 42% to 74%.

3.3.2 Nanorod length

The optimal wavelengths as a function of nanotip length are plotted in Figure 7, along with linear trendlines. When adjusting the length of the nanotip, a strong linearity of the shift of the optimal wavelengths was formed. These points are red-shifted (the wavelengths increase) as the tip length increases, and follow the equations below

$$\lambda_{abs} = 0.8342\ell + 265.14 \quad (3.8)$$

$$\lambda_{refl} = 0.8148\ell + 292.94 \quad (3.9)$$

$$\lambda_{trans} = 0.7447\ell + 350.73 \quad (3.10)$$

These trendline equations yield residual-squared values of 0.9890, 0.9917, and 0.9893, respectively. The reflectance increases from 1.6 to 2.2%, the transmittance is maintained around 46.6%, and the absorbance is maintained at around 53%. The cause for the red shift of the optimal wavelengths is dependent on the size of the tip. When a wave propagates through the metal tip, a standing wave forms whose wavelength dependent on the length of the tip. As that length increases, longer wavelengths of light exist inside it.

3.3.3 Nickel film thickness

A plot optimized wavelengths as a function of nickel film thickness can be seen in Figure 8. Comparing the thickness of the nickel film underneath the nanotip in this figure, there is a strong increase of the optimized wavelengths from 0 to 40 nm thickness—624 nm for minimum reflectance, 648.4 nm for maximum transmittance, and 604.4 nm for maximum absorbance. Thicker than 40 nm, the optimized wavelengths level off to 618.7 nm for minimum reflectance, 647 nm for maximum transmittance, and 598.9 for maximum absorbance. Between 0 and 120 nm nickel thickness, the reflectance increases from 0.07 to 1.9%, the absorbance decreases from 59.42 to 53.13%, and the transmittance increases from 40.6 to 46.4%. The optimal wavelengths stay the same above 40 nm nickel thickness because then the nickel acts less like a thin film and more as just a surface. Alterations of the optimal wavelengths occur because of changes to the surface-to-volume ratio; however, when the nickel film is greater than 40 nm thick, the nickel acts as a bulk. Much of this has to do with penetration depth of the light which is dependent on

the wavelength of light. In this instance, exposed silicon will have maximum transmittance at about 600 nm, but with a 20 nm-thick film of nickel on top, the wavelength of maximum transmittance would increase to 640 nm.

3.3.4 Silver apex film thickness

Figure 9 plots the optimal wavelength as compared to the silver apex film thickness along with linear trendlines. Varying the thickness of the silver film on the apex from 22 to 38 nm yields a blue-shift model that is also strongly linear. They, too, follow

$$\lambda_{abs} = -1.9719t + 657.44 \quad (3.11)$$

$$\lambda_{refl} = -1.8978t + 675.57 \quad (3.12)$$

$$\lambda_{trans} = -1.7966t + 702.44 \quad (3.13)$$

These trendline equations yield residual-squared values of 0.9999, 0.9999, and 0.9991, respectively. When increasing the silver thickness from 22 to 38 nm, the reflectance maintains 2%, the absorbance maintains 52%, and the transmittance maintains 46%. Notice the slopes of these trendlines are negative which suggests an increase in silver will cause the optimal wavelengths to decrease. The cause of the blue-shift is dependent on the amount of silver available. As the thickness of silver increases, the electrons have more space to oscillate more freely (compared to the nickel). Since there is more space to move, they will resonante at a larger frequency and thus a smaller wavelength—towards the blue.

With the given models, it is now possible to fabricate a substrate of nickel nanorods to optimize a particular wavelength for either absorbance or reflectance. For instance, perhaps a particular setup requires a laser that is 633 nm wavelength. With the information from the simulations, one can determine specific dimensions the nickel nanotips could have to maximize

the amount of absorption. The length of the nickel nanotip would be 440 nm, the width would be 120 nm, the nickel thickness would need a minimum of 50 nm, and the silver layer on the apex would be 39 nm. If a Raman scattering experiment were using a 633 nm laser, a nickel nanorod film with the specifications above could be fabricated and used for SERS. Since these specifications allow for a maximized absorption at 633 nm wavelength, the substrate should produce a strong surface plasmon that would enhance the vibrations of the molecules being probed.

Chapter 3 Figures

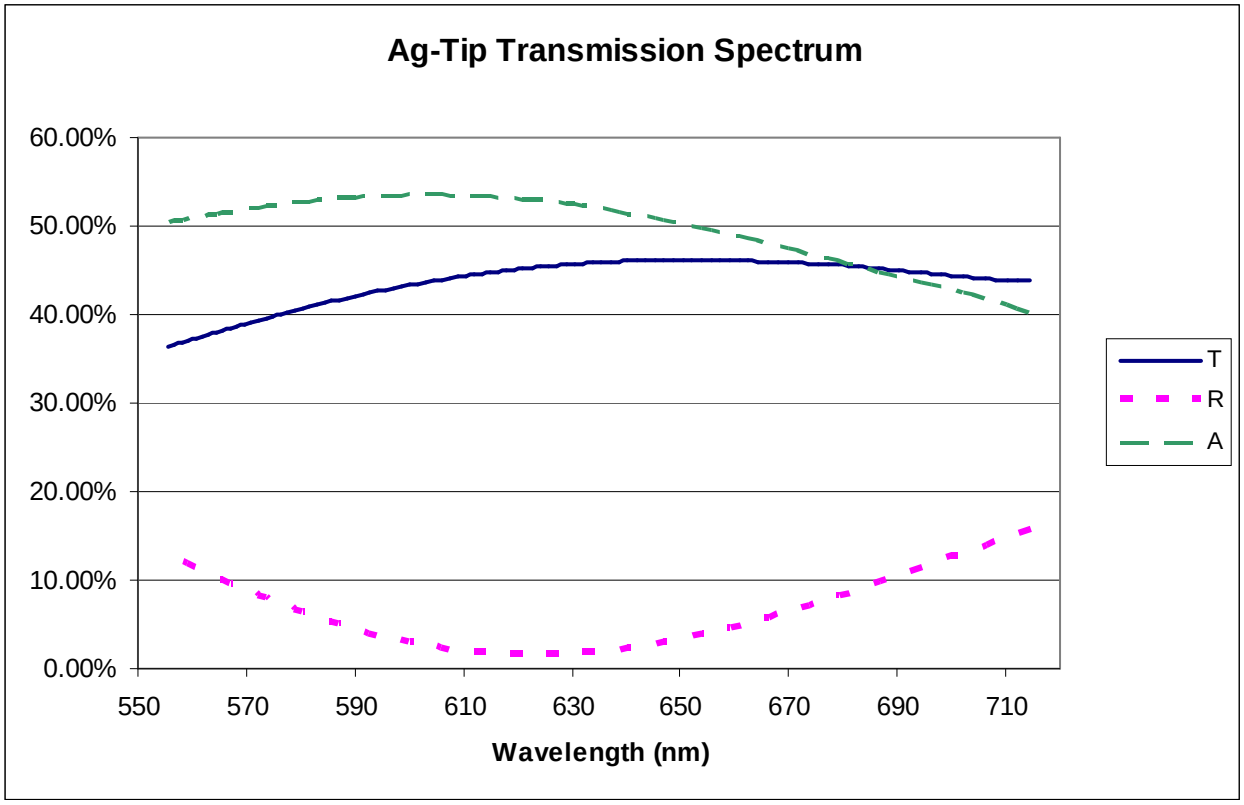

Figure 5: A typical absorption-reflection-transmission spectrum for the nickel nanotip with silver thin film. The main features include a minimum for the reflectance, as well as maximum values for both transmission and absorption.

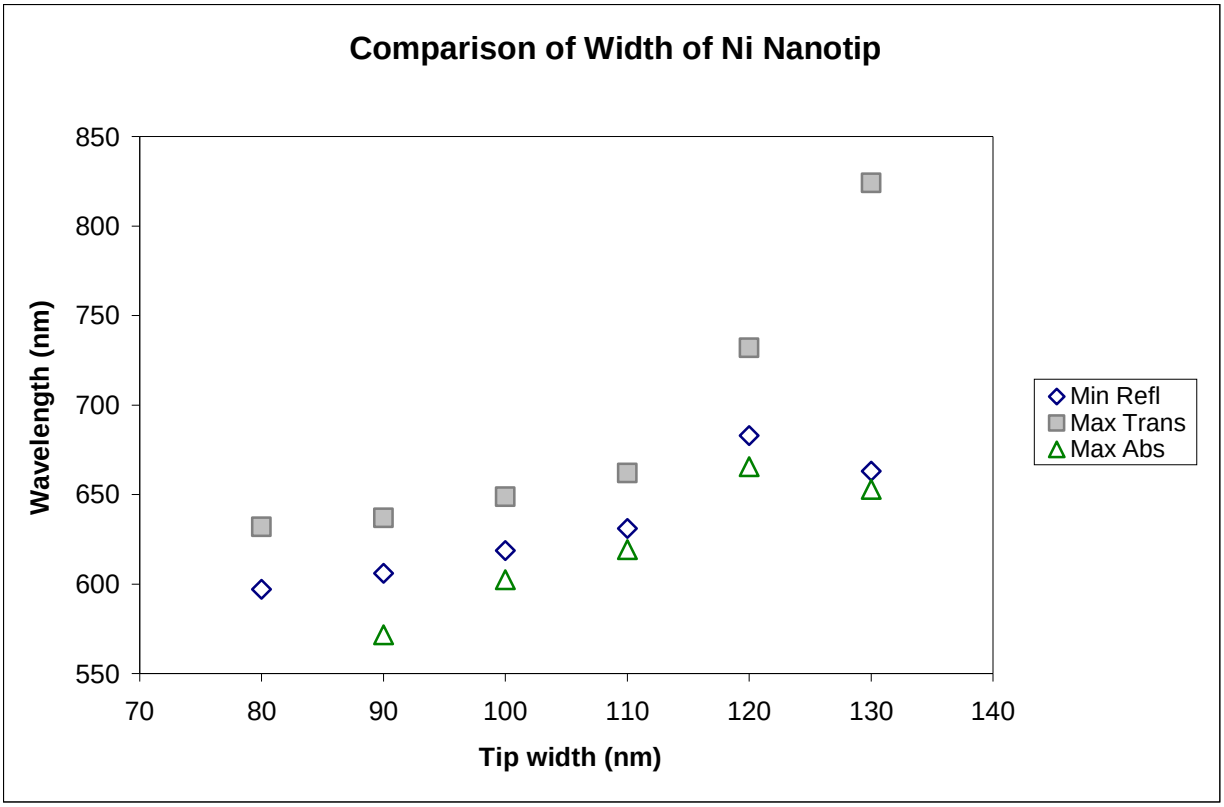

Figure 6: Optimized wavelengths vary with the width of the nickel nanotip.

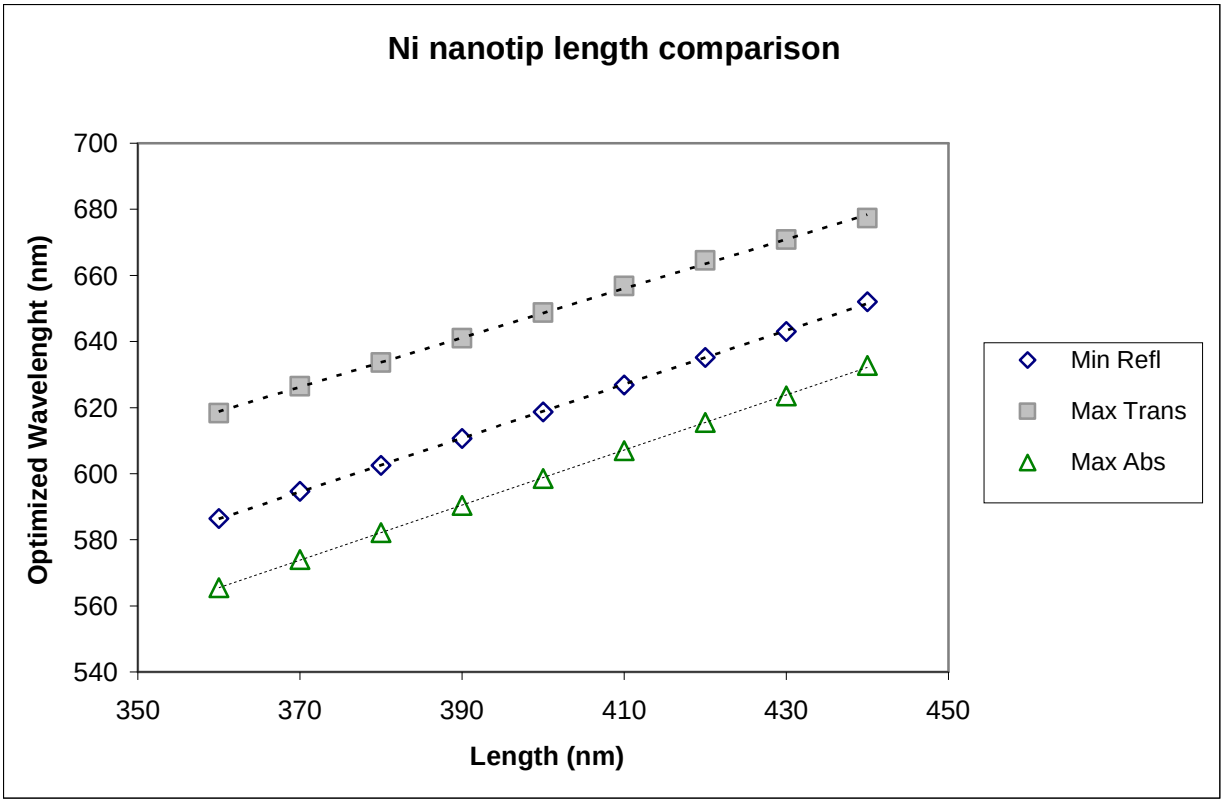

Figure 7: Optimized wavelengths for varying nanotip length.

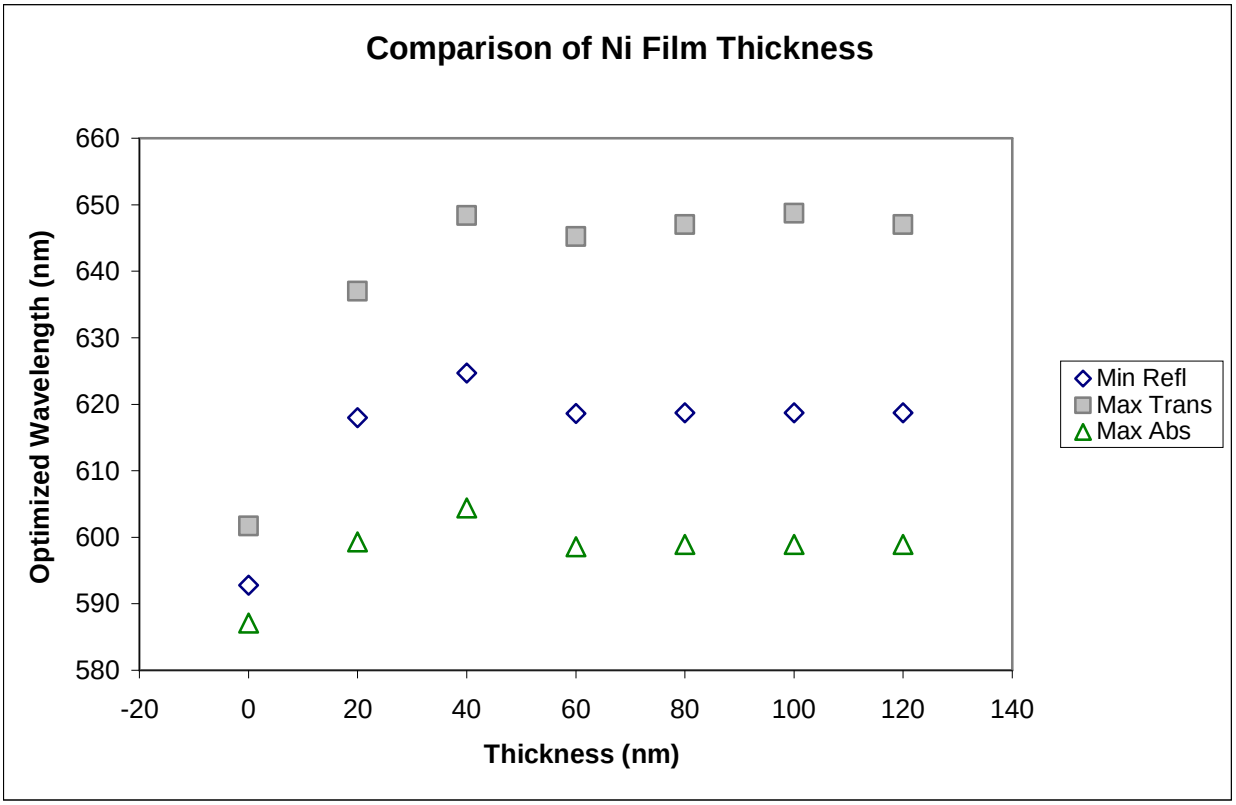

Figure 8: Optimized wavelengths for varying thickness of the nickel film beneath the nanotip.

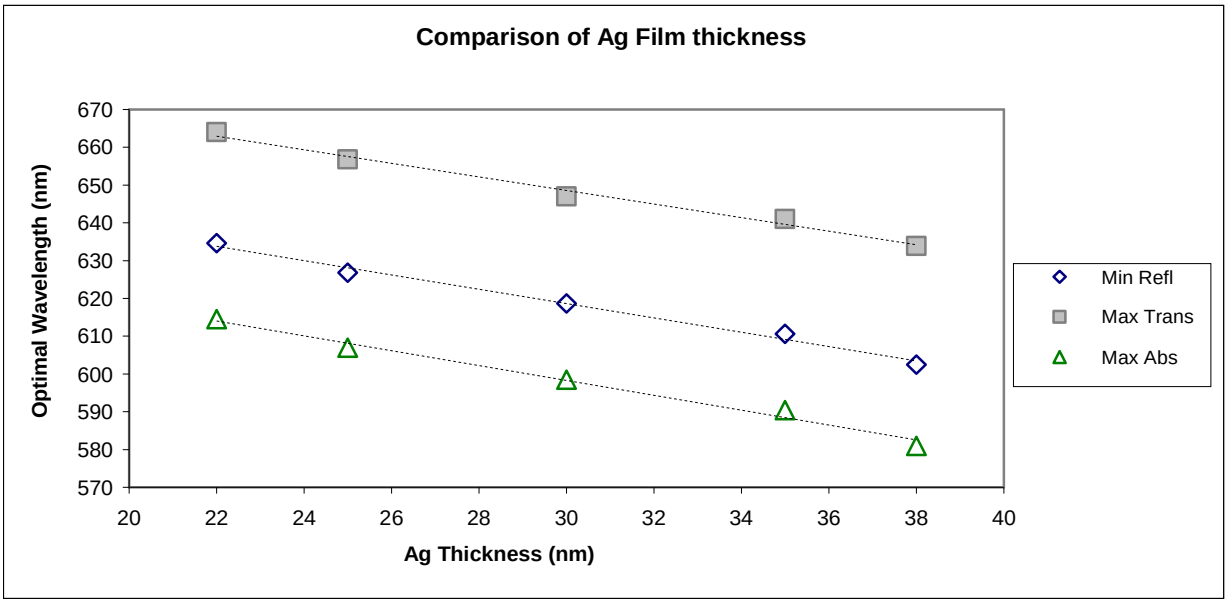

Figure 9: Optimal wavelengths vary with silver film thickness on the apex.

4. Electric Field Localization and Enhancement

As it was mentioned before, when the electromagnetic wave propagates onto metal structures, the electrons inside will oscillate with the incoming wave. This oscillation yields strong electric fields particularly on the surface of the structure. Since our metallic structure is a long tip, the electric field concentration should be very strong[33]. The following section will discuss the procedure and results of simulating the electric field localization around the tip by the FDTD method.

4.1 Field Localization setup

The geometries and optical properties for the nickel nanotips are the same as before. The source for this procedure will be that of a plane wave, polarized in both y- and z-axes (orthogonal to the length of the tip). The wavelengths focused in this simulation are 532, 572, and 633 nm. The plane wave will have an amplitude function built in so that the incident angle of the light can be altered. This involves the equation

$$f(r) = e^{-i\vec{k}\cdot\vec{r}}, \qquad (4.1)$$

where $\vec{k}$ is the wavenumber that is dependent on the wavelength and $\vec{r}$ is the distance across the plane of the source. This function allows the amplitude of the wave function to fluctuate across the plane of the source which will yield a plane wave that is tilted. Figure 10 shows the plane

wave propagating at the angles 30, 45, and 60 degrees, whereas the blue denotes a positive z-direction electric field, the red denotes a negative z-direction electric field, and the arrows denote the direction of the plane wave.

In order to visualize of the localized fields, Meep is ran with a continuous, plane-wave source with polarization in both y- and z- axes (perpendicular to the nanorod) for the specified wavelengths, metal coatings, and angle of the incident light onto the general nickel nanotip structure. The values of the fields in all three directions are stored in a HDF5 file, essentially a large matrix that allows data (in this case, for the fields) for all three dimensions over time. When the simulation is done, the program "h5tovtk" (from h5utils, version 1.12.1, developed by Steven G. Johnson, MIT) will be applied to convert the multidimensional file into a VTK file[34]. The VTK file will then, in turn, be read by Mayavi (version 3.4.1), a software package that allows the 3D visualization of data[35].

The images presented in this section will be of an isotropic view of the tip. The images will also be showing the intensity of the field,

$$I = \vec{E}^{*}\vec{E} = E_x{}^{*}E_x + E_y{}^{*}E_y + E_z{}^{*}E_z \tag{4.2}$$

where the intensity is the sum of the electric field in Cartesian coordinates multiplied by its complex conjugate.

4.1.1 Metal Comparison

Investigating the differences of localization between metals, the excitation wave was set for the simulation with a wavelength specified at 572 nm with 45° linearly-polarized light in both y- and z-directions. The reason for the polarity at 45° is that the electric field at this angle would move charges to opposing corners of the tip instead of opposing sides. This would increase the charge

density on the tip considerably in order to maximize enhancement. Figure 11 displays the tip as well as the electric field intensity between (a) silver, (b) gold, and (c) nickel. Between the different metals, it appears as if the localizations are identical—there is strong localization at opposing corners, as suggested before, forming a dipole. There is localization along the shaft of the tip, which suggests that the nickel surface acts as a waveguide for these surface plasmons. Observing these localizations over time, the apex localization remains stationary for some time, and at some point will start propagating down the nickel towards the nickel film substrate and repeat the process again.

4.1.2 Wavelength Comparison

In order to investigate the differences of localization between excitation wave wavelengths, the apex layer was set to silver, and the source was set to have normal incident light with 45° linearly-polarized light. Figure 12 display the tip and the electric field localization of (a) 532 nm, (b) 572 nm, and (c) 633 nm wavelengths of light. In this figure, the gradient of the field is different for each wavelength; the field is spread out more for 572 nm wavelength than for 532 and 633 nm. The image (b) shows a field that is both localized and more spread out compared to image (c), suggesting that the charge is concentrated greater at that point, whereas image (a) has its field moving toward the substrate, suggesting the localized plasmon is beginning to migrate toward the base. Localization occurs on the corners of the apex, as well as the localization propagating downward, as was seen in Section 4.1.1.

4.1.3 Incidence Angle Comparison

To compare the differences between the incident angles of the excitation source, the wavelength was established at 572 nm, and the metal layer on the apex was set to silver. Figure 13 shows the

tip as well as the electric field intensity dependent on (a) normal incidence, (b) 30° incidence, (c) 45° incidence, and (d) 60° incidence light. When the electric field for different source angles was visualized, the localization changes drastically—while the field is localizing at the same opposing corners of the apex, the intensity of the field drops dramatically once the source's angle changes to 30. Increasing the angle of light, the localization becomes less symmetric and less intense. The scale on the side of these images is drastically large in relation to the contours of the localization on the tip. This is due to the source producing a very strong electric field compared to the rest of the cell.

4.2 Enhancement factor

As was mentioned before, there is interest in the enhancement of the electric field caused by localized surface plasmons. The electric field localizes along the edges of the apex, so now a quantitative analysis will be performed in order to determine how strong this field is over time. There will be an intuitive analysis of how the electric field changes along the dielectric interface of the nickel nanotip. A comparison between metals films (silver, gold, and nickel) will be studied, as well as a comparison of the different source wavelengths (532, 572, and 633 nm).

The enhancement will be defined as the ratio between the electric field with the tip and the electric field without the tip, such that

$$Enh = \frac{\left|\vec{E}_{tip}\right|}{\left|\vec{E}_{o}\right|} = \sqrt{\frac{\vec{E}^{*}_{tip}\vec{E}_{tip}}{\vec{E}^{*}_{o}\vec{E}_{o}}} \qquad (5.1)$$

In this equation, the electric field is multiplied by its complex conjugate (since the electric field is time dependent, and thus complex due to its plane wave form from Eq 1.3).

4.2.1 Enhancement Simulation and Calculation

The dielectric model will be consistent with what was described in previous sections. The only alteration is the variation of the thin layer of metal on the apex of the tip; the metal selection will be gold, silver, and nickel (as if to simulate nickel nanotips without a special metal coating).

The wavelengths 532, 572, and 633 nm will be used with normal incidence light. The source will be of normal, continuous plane waves that are 45° linearly polarized as was used in the simulations mentioned previously.

It is first important to note where the highest intensity due to the localized surface plasmon resonance lies along the surface of the tip. The last chapter allowed us to visualize where the strongest fields are located, which were, for the most part, on two opposing corners. To calculate the enhancement due to the nickel nanotip, it is necessary to pinpoint where the field is strongest on the tip. The positions and coordinates of the five test points are identified in Figure 14 as a top-down image of the tip. The coordinate system, derived from Meep, is based on a corner of the cell above the tip and source. The graphs of Figure 15 demonstrate the strength of the electric field intensity along the x-axis at given points in the y-z plane for both 572 and 633 nm wavelength. The greatest intensity for each test location was determined by choosing the strongest intensity out of a small range of time. The intensity is greatest at a point (68, 5, 5) for both 633 and 572 nm wavelengths; the enhancement will be probed at that particular point in the simulation for the rest of this study.

The enhancement is calculated as a function of time, where time is started when the simulation begins. The enhancement fluctuates over time (since it is a surface charge density wave) on the order of femtoseconds; at particular times along this range the enhancement will be

the highest. The graphs in Figures 16-18 are scaled down from the full 40 fs range to concentrate on a small time frame where the maximum enhancement occurs.

4.2.2 Enhancement Dependent of Wavelength

The enhancement with 532 nm light in Figure 16 shows that silver has the least enhancement of the three (2.804×10^7 at 23.28 fs). Nickel and gold have nearly equivalent enhancements (8.277×10^7 at 23.28 fs and 9.501×10^7 at 23.2 fs, respectively).

The enhancement with 572 nm light in Figure 17 shows that gold has the strongest maximum enhancement (8.732×10^4) with nickel less (3.283×10^4) and silver the least (2.6135×10^3); the peak of all these enhancements occur at 36.9 fs. Note, however, that the nickel has the lowest minimum enhancement, which shows that it has a very large change in enhancement compared to the other two metals.

Enhancement with 633 nm light in Figure 18 shows that silver has the strongest maximum enhancement (9.353×10^4) of the three metals. Nickel shows the second strongest maximum enhancement (1.920×10^4) with gold having the smallest maximum enhancement (4.9282×10^3) within the time frame of 20 to 25 fs. These maximum enhancements occurred at 22.96 fs into the simulation. It is important to point out that silver has the smallest minimum enhancement, thus showing that there is large differentiation in the enhancement with silver. Another interesting feature of the 633 nm enhancement is that gold has a strong enhancement (1.998×10^4) towards the beginning at 2.08 fs.

The peculiarity is that normally gold nanoparticles absorb more light with longer wavelengths (approximately 520 nm) and silver nanoparticles absorb more light with shorter wavelengths (approximately 390 nm) [36]. This simulation showed, however, that silver has higher enhancement near the 633 nm wavelength and gold has a higher enhancement near 532 nm

wavelength. Keep in mind that gold did peak earlier than the other two maximum enhancements in 633 nm, and within the same order of magnitude. Because of this, gold is still the dominant enhancement metal for this frequency range. A survey of near UV wavelengths (450 to 200 nm) is expected to show a large enhancement for silver.

Chapter 4 Figures

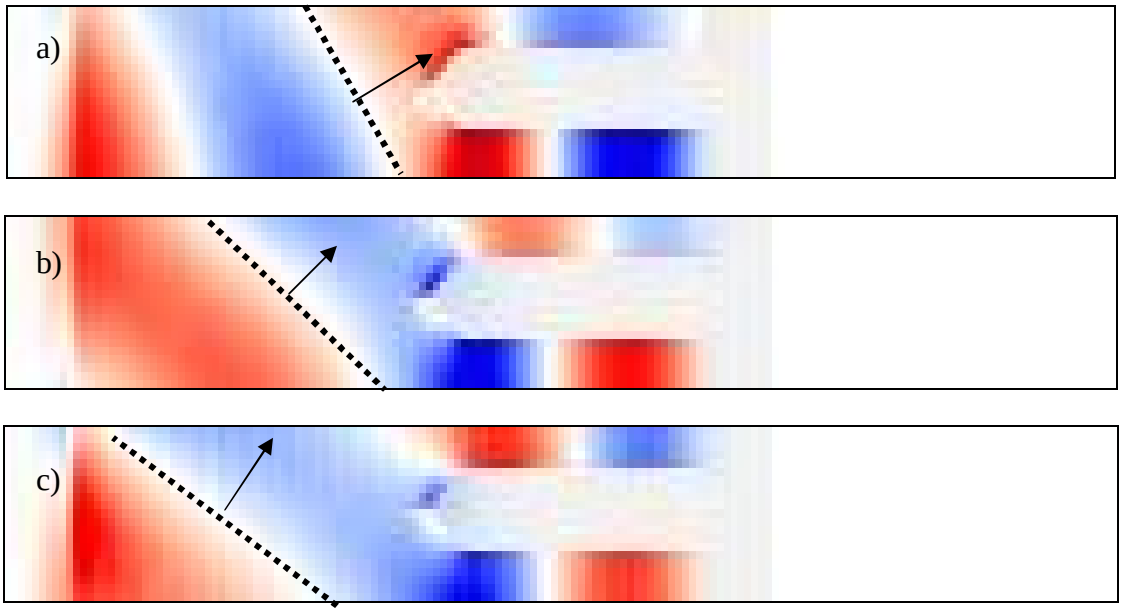

Figure 10: Electromagnetic plane wave impinging onto the nanotip with the incident angles a) 30^{o}, b) 45^{o}, and c) 60^{o} from normal.

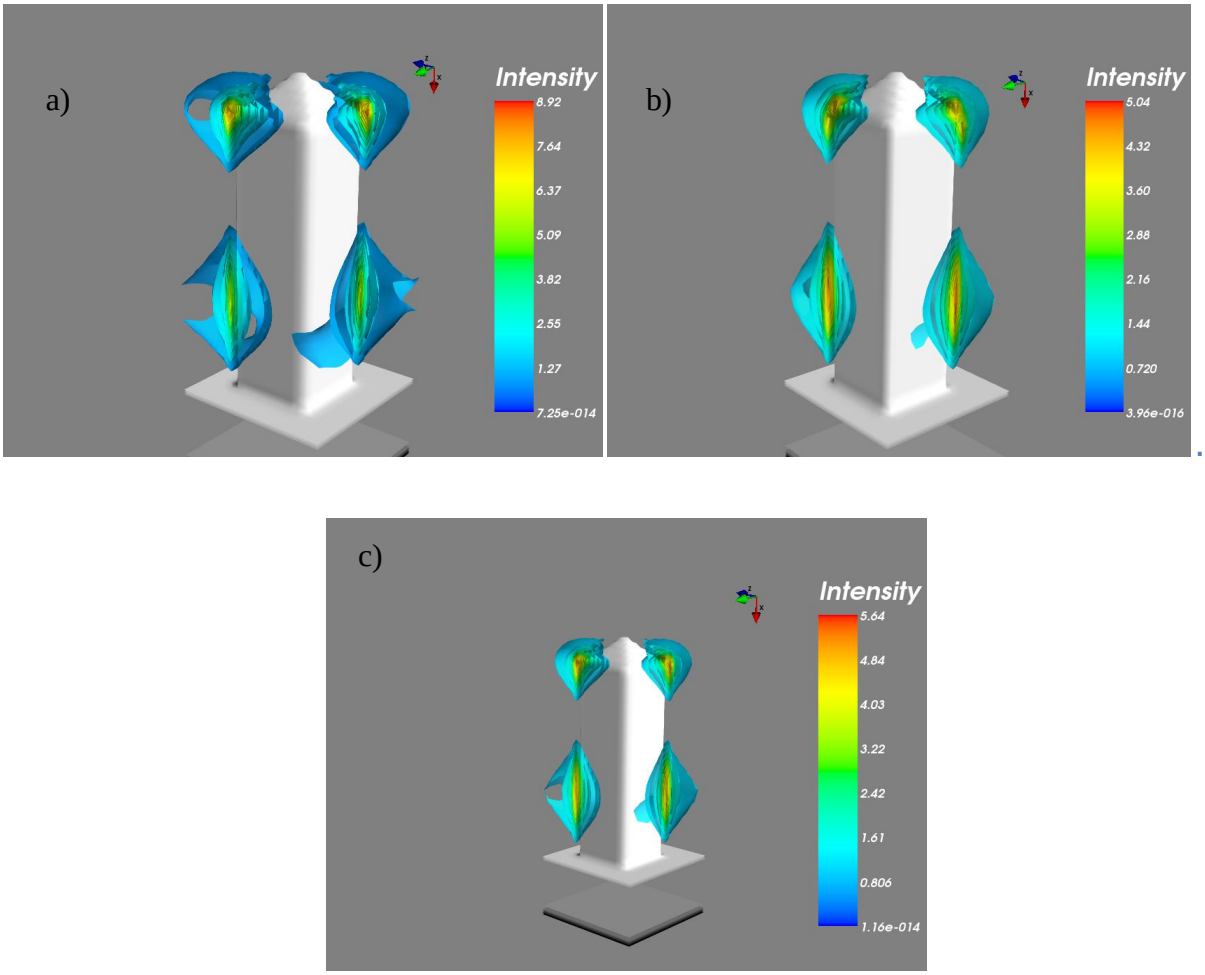

Figure 11: Light localization dependent on 30 nm metal film, with 572 nm normal incidence light, 45° linearly polarized. a) silver, b) gold, c) nickel.

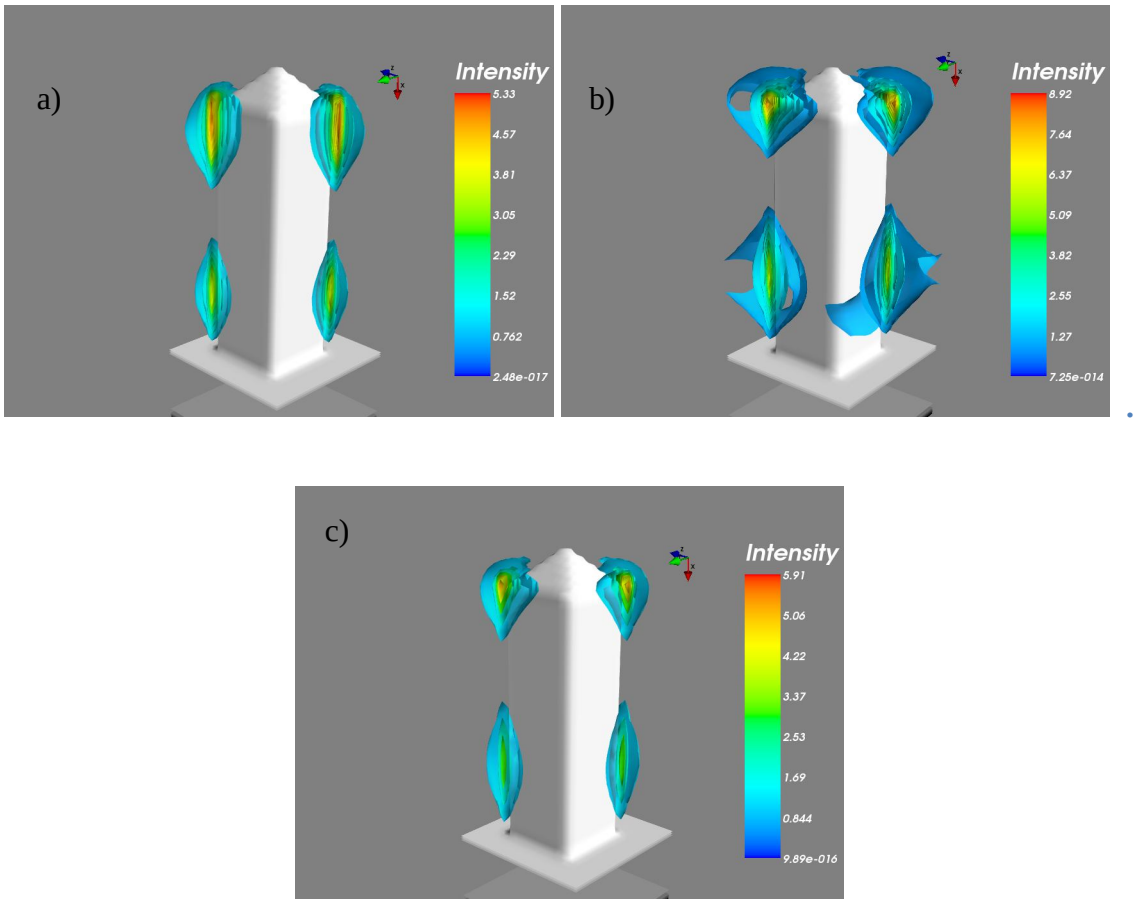

Figure 12: Localization dependent on wavelength of light, normal incidence, 45° linearly polarized, with 30 nm silver film. a) 532 nm, b) 572 nm, c) 633 nm.

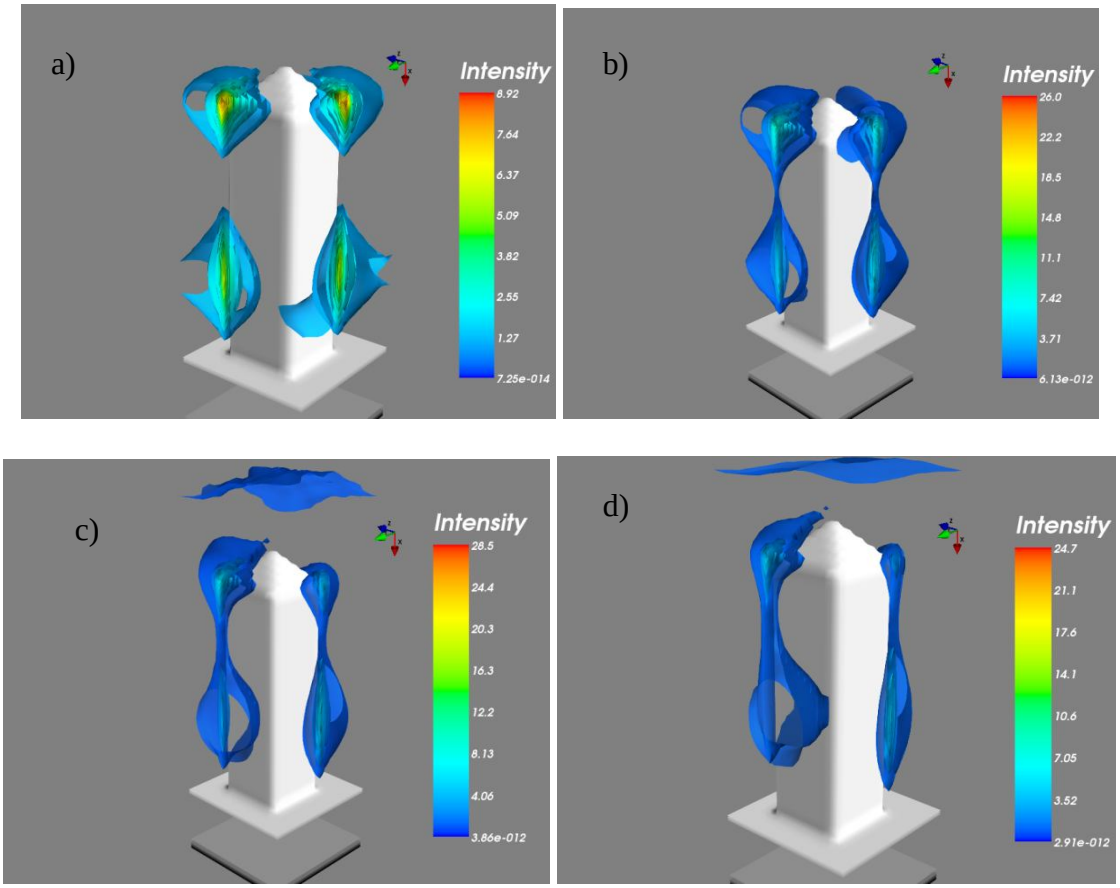

Figure 13: Localization dependent on incidence angle, with 30 nm silver thin film, 572 nm wavelength, 45° linearly-polarized light. a) Normal incident light, b) 30^{o} incident light, c) 45^{o} incident light, d) 60^{o} incident light

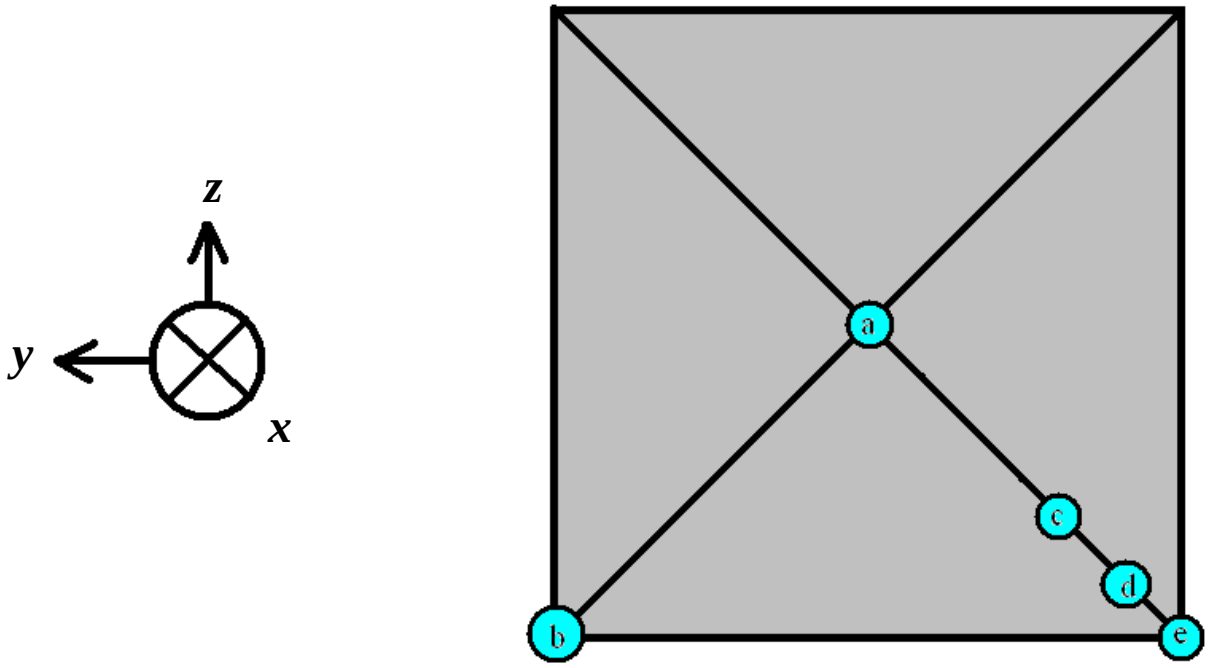

Figure 14: The test points for calculating enhancement for the nickel nanotip, a) (11, 11), b) (5,14), c) (7,7), d) (6,6), e) (5, 5).

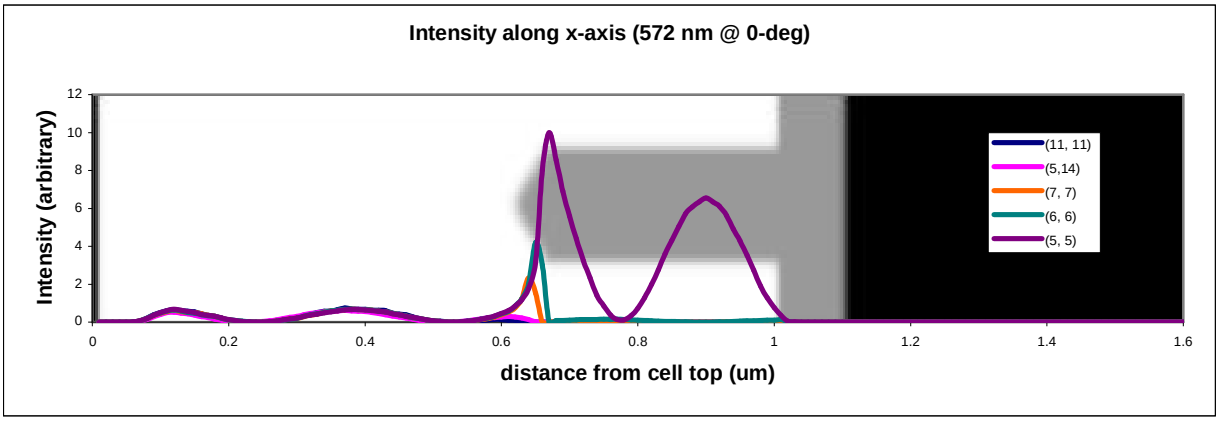

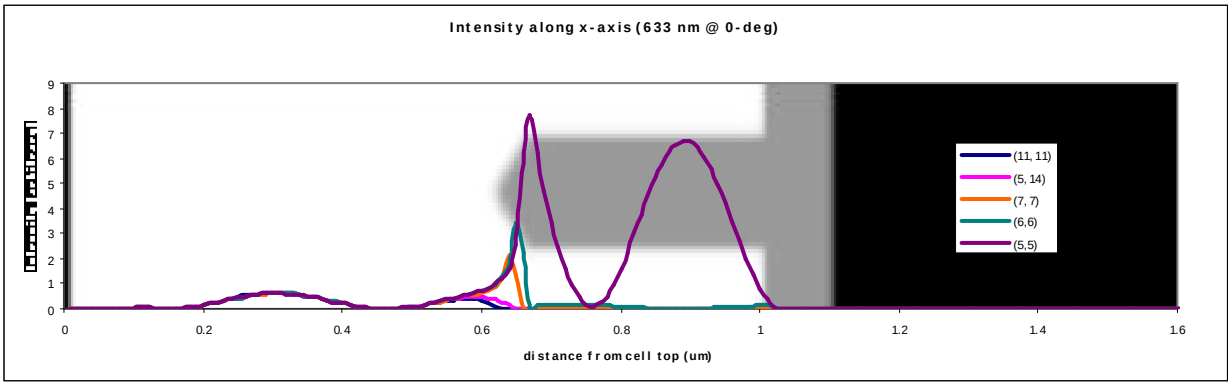

Figure 15: Intensities along the x-axis at various y-z coordinates. These charts show how the strong the field is along the x-axis at various points. It proves that the strongest fields on the tip are at the base of the apex.

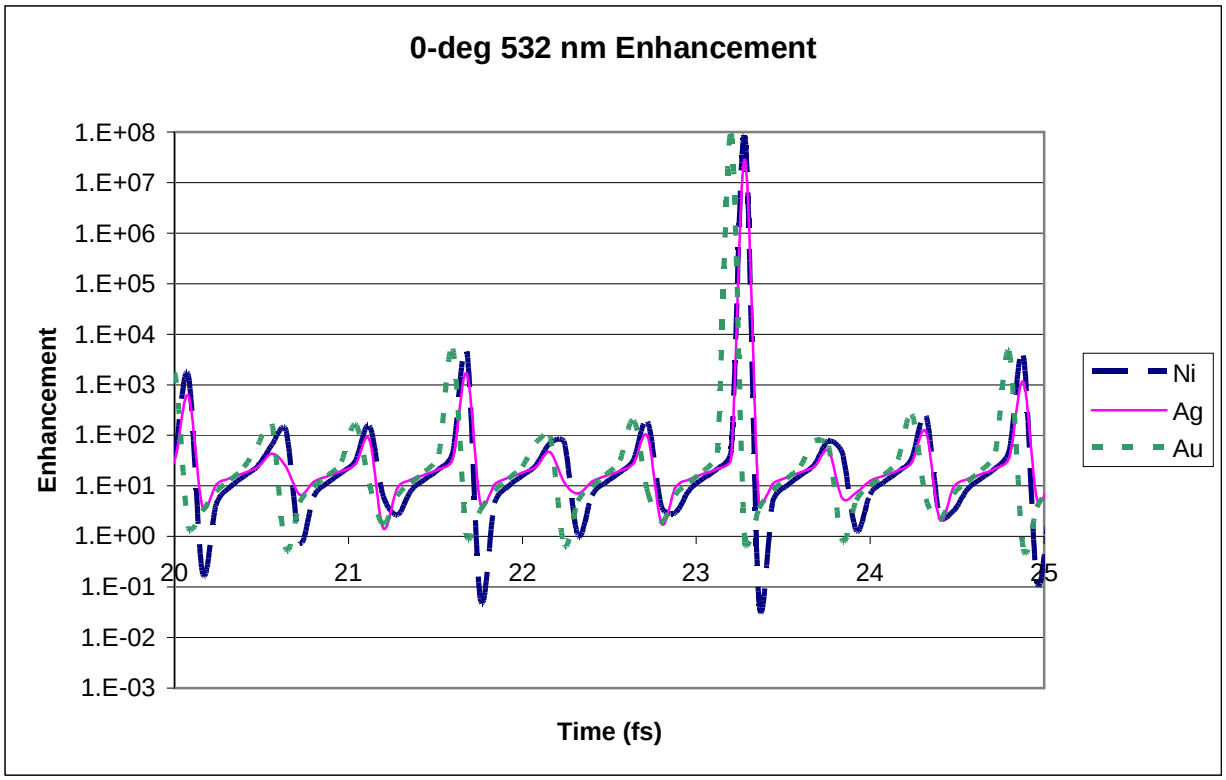

Figure 16: Enhancement with normal-incident, 45° linearly-polarized light with 532 nm wavelength at the apex corner between 20 and 25 fs.

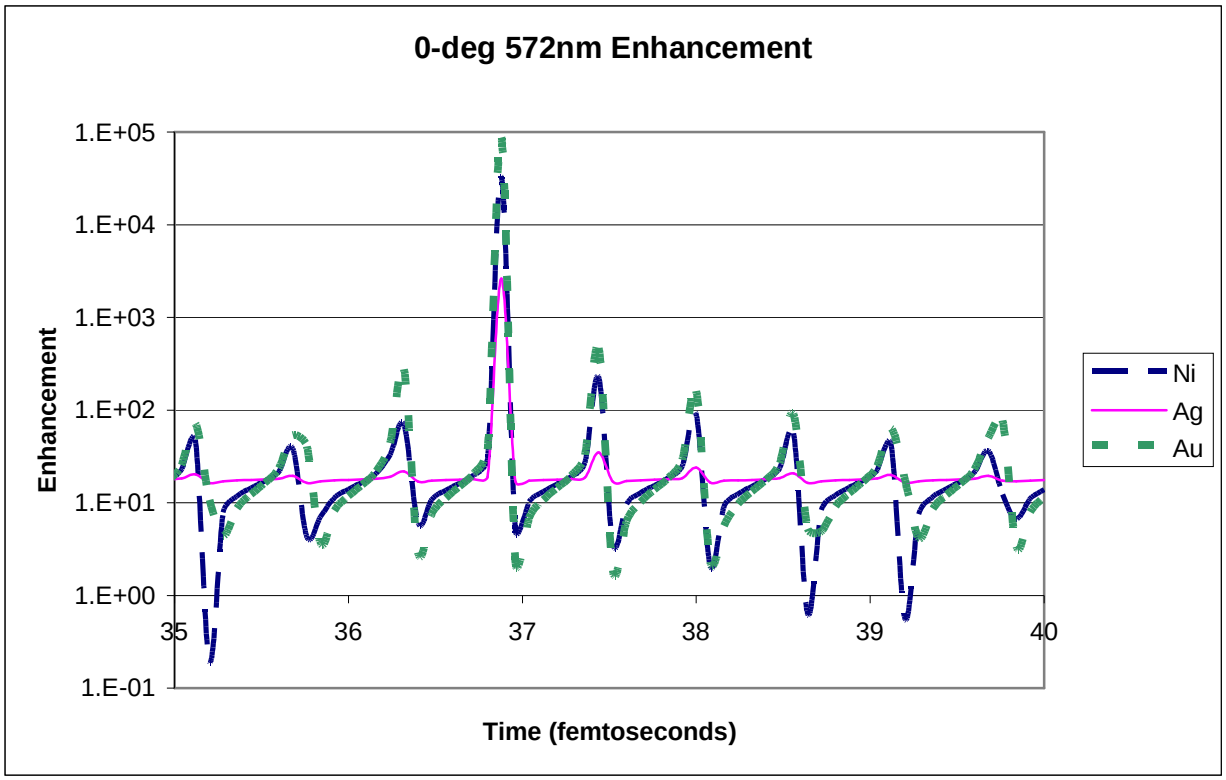

Figure 17: Enhancement with normal-incident, 45° linearly-polarized light with 572 nm wavelength at the apex corner between 35 and 40 fs.

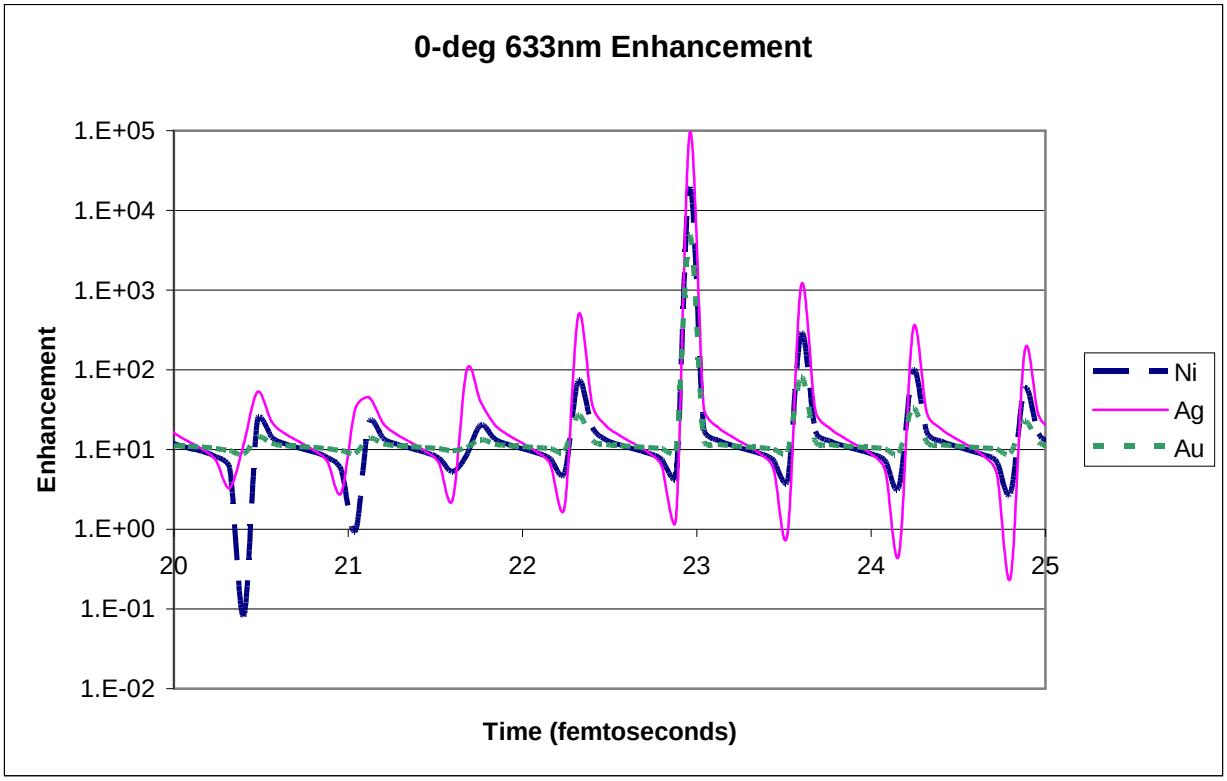

Figure 18: Enhancement with normal-incident, 45° linearly-polarized light with 633 nm wavelength at the apex corner between 20 and 25 fs.

5. Conclusion

5.1 Summary

In summary, the finite-difference time-domain method was applied to model electromagnetic properties of nickel nanotips via Meep. The reflectance, absorbance, and transmittance of these nanotips were calculated, and the dimensions were varied to determine the wavelengths of the minimum reflectance, maximum transmittance, and maximum absorbance. The intensity of the electric field around the tip was visualized to determine where the localization of the field existed around the tip. Lastly, the enhancement of the electric field was calculated at the strongest intensity coordinate of the localization, comparing both wavelength and metal film on the apex.

Error is possible in these simulations. One source of error in these simulations is due to resolution size. In these simulations, the resolution was set at $1/10^{th}$ of a unit cell, or 10 nm. As in many computational processes, a tradeoff exists between higher resolution and computational power (which translates to amount of time spent simulating this process). A larger resolution would yield results that would better approximate the field calculations, but would require much more time to compute. For instance, twice the resolution would require the simulations to perform eight times the number of calculations to account for volume.

Another source of error could be the PML layer. Recall that the PML is used to prevent light from reflecting off a cell wall or allow it to be transmitted—a fully absorbing wall.

Generally the PML needs to be approximately one wavelength wide[28]. In Chapter 3, however, the simulation required a spectrum of wavelengths used that would either be too shot or too long compared to the PML. Not only this, but larger PML requires larger computational cells which would require more computational power. Since these methods require multiple simulations for data, the PML in these simulations were reduced in an effort to reduce the amount of time.

Lastly, the positions of the detector planes from Chapter 3 could be sources of error. For instance, if the transmission detector was placed right at the nickel-silicon interface, the majority of the absorption would be due to plasmons. The reflection detector could be further away from both the apex and the source, but due to period cell boundaries this might not do much. If part of the wave was reflected off the object at an angle away from the normal, it would simply pass through one cell wall and reappear through the opposing wall.

5.2 Investigation of Angle-dependent Enhancement

This investigation of the enhancement can continue further if one wants to consider the dependence of the enhancement with a varying incident angle of the excitation wave. When the enhancement with a tilted excitation source was calculated, there was a major decrease in enhancement from normal incident light to 30^{o} by five or six orders of magnitude, which is something that should not be seen—since the same intensity source is incident onto a slightly different angle, the enhancement should be about the same. This was also discussed in Section 4.1.3 where the field localization was weakly oscillating. It is possible that the formulation of the tilted plane wave is flawed. Meep programming favors shapes that are orthogonal such as prisms, cones, and cylinders; it is a common issue for users to have trouble setting up a proper tilted plane wave for simulations[37]. Although it was shown that the simulation used here

developed a proper angle (Figure 10), it is possible that the amplitude of the wave decreases drastically to account for this discrepancy.

5.3 Experimental Verification

Many of these models can be verified through experimental means. For instance, creating a sample of silver-coated nickel nanotips onto a Si substrate and then using either UV-Visible or Attenuated Total Reflection spectroscopy to measure the amount of reflectivity should be comparable to these results. Also, another way to test these simulations would be to fabricate a nickel nanorod thin film that would maximize the absorbance to then use it for SERS as a comparison to a thin film that uses the base dimensions in these simulations to see if the sensitivity is increased, as was explained at the end of Chapter 3.

5.4 Prospective Projects

Besides correcting the tilted plane waves, there is much to be continued on this project. While gold and silver are impressive metals when containing surface plasmons, it can be quite expensive. Other metals, chiefly copper, could be used as a cheaper alternative for the thin apex layer or as the entire tip. Optical properties from Rakic *et al.* could be modeled in Meep and compared to see if the enhancement of the field would be beneficial.

Appendix A: Meep Control File

```
;;reset all parameters of Meep
(reset-meep)
;;define specific lengths
(define-param a (/ (sqrt 2) 2))
(define-param b (* (sqrt 2) 0.05))
;;define optical properties of metals
(define Au (make dielectric (epsilon 1)
(polarizations
 (make polarizability
(omega 1e-20) (gamma 0.0042747) (sigma 4.03e+39))
(make polarizability
(omega 0.03347) (gamma 0.019438) (sigma 11.3629))
(make polarizability
(omega 0.06694) (gamma 0.027826) (sigma 1.18364))
(make polarizability
(omega 0.23947) (gamma 0.070170) (sigma 0.65677))
(make polarizability
(omega 0.34714) (gamma 0.201155) (sigma 2.64548))
(make polarizability
(omega 1.07433) (gamma 0.178571) (sigma 2.01482))
)))
(define Ni (make dielectric (epsilon 1)
(polarizations
 (make polarizability
(omega 1e-20) (gamma 0.0038715) (sigma 1.5828e+39))
(make polarizability
(omega 0.014034) (gamma 0.36384) (sigma 837.12))
(make polarizability
(omega 0.046941) (gamma 0.10759) (sigma 101.01))
(make polarizability
(omega 0.12881) (gamma 0.17567) (sigma 10.534))
(make polarizability
(omega 0.49111) (gamma 0.50748) (sigma 4.9834))
)))
(define-param no-tip? false)

;;create the lattice cell
(set! geometry-lattice (make lattice (size 16 2 2)))
;;set up the dielectrics
(set! geometry
;;for no tip (blank cell)
            (if no-tip?
              (list (make block (center 5.5 0 0) (size infinity infinity
infinity)
                 (material air)))
;;for the tip (filled cell)
              (list
```

```
;;Insert a layer of nickel film
              (make block (center 2.5 0 0) (size 1 infinity infinity)
               (material Ni))

;;silicon substrate
               (make block (center 5.5 0 0) (size 5 infinity infinity)
                 (material (make dielectric (epsilon 12))))

;for fitted nickel


             (make block (center 0 0 0) (size 4 1 1)
              (material Ni))

;Silver coat on the tip
                (make block (center (- b 1.75) (+ -1.75 b) 0)
                 (size (+ 0.2 (* 0.5 (sqrt 2))) 0.2 1)
                 (e1 1 1 0)
                 (e2 -1 1 0)
                 (e3 0 0 1)
                 (material Au))

                (make block (center (- b 1.75) (- -2.25 b) 0)
                 (size (+ 0.2 (* 0.5 (sqrt 2))) 0.2 1)
                 (e1 1 -1 0)
                 (e2 -1 -1 0)
                 (e3 0 0 1)
                 (material Au))

                (make block (center (- b 1.75) 0 (+ -1.75 b))
                  (size (+ 0.2 (* 0.5 (sqrt 2))) 1 0.2)
                  (e1 1 0 1)
                  (e2 0 1 0)
                  (e3 -1 0 1)
                  (material Au))

                (make block (center (- b 1.75) 0 (- -2.25 b))
                  (size (+ 0.2 (* 0.5 (sqrt 2))) 1 0.2)
                  (e1 1 0 -1)
                  (e2 0 1 0)
                  (e3 -1 0 -1)
                  (material Au))
;; use air block to cut pyramid
              (make block (center -2 0.5 0)
                (size a a 1)
                (e1 1 1 0)
                (e2 -1 1 0)
                (e3 0 0 1)
                (material (make dielectric (epsilon 1))))

               (make block (center -1 0.65 0)
                 (size 4 0.2 1)
                 (material (make dielectric (epsilon 1))))

               (make block (center -2 -0.5 0)
```

```
                  (size a a 1)
                  (e1 1 -1 0)
                  (e2 -1 -1 0)
                  (e3 0 0 1)
                  (material (make dielectric (epsilon 1))))

                (make block (center -1 -0.65 0)
                  (size 4 0.2 1)
                  (material (make dielectric (epsilon 1))))

                (make block (center -2 0 0.5)
                   (size a 1 a)
                   (e1 1 0 1)
                   (e2 0 1 0)
                   (e3 -1 0 1)
                   (material (make dielectric (epsilon 1))))

                (make block (center -1 0 0.65)
                  (size 4 1 0.2)
                  (material (make dielectric (epsilon 1))))

                (make block (center -2 0 -0.5)
                   (size a 1 a)
                   (e1 1 0 -1)
                   (e2 0 1 0)
                   (e3 -1 0 -1)
                   (material (make dielectric (epsilon 1))))

                (make block (center -1 0 -0.65)
                  (size 4 1 0.2)
                  (material (make dielectric (epsilon 1))))

                )))

;;Develop the EM source for tilted angle.
(define-param fcen .1748)   ;    fcen = .196 633nm=0.1580 572nm=0.1748
(define-param df 0.0001)
;;set up the tilted EM source
(define theta (* 0 (/ pi 180)))
(define k (* fcen (sin theta)))
(set! k-point (vector3 0 0 k))
(define (my-amp-func p) (exp (* 0+2i pi k (vector3-z p))))
(set! resolution 10)
(set! eps-averaging? false)
;;Place sources
(set! sources (list
;;Z-polarized wave
                (make source
                     (src (make continuous-src (frequency fcen)))
                      (component Ez)
;                      (amp-func my-amp-func)
                      (center -7 0 0)(size 0 2 2)
                )
;;Y-polarized wave
                (make source
                      (src (make continuous-src (frequency fcen)))
                       (component Ey)
```

```
                    (center -7 0 0) (size 0 2 2)
                )
))
;;extablish Perfectly-matched layer (PML)
(set! pml-layers (list (make pml (direction X) (thickness 1))))
;;Determine the intensity function
(define (E2)
  (output-field-function "E-mag" (list Ex Ey Ez)
   (lambda (r ex ey ez)
  (+ (+ (* ex (conj ex)) (* ey (conj ey))) (* ez (conj ez))))))
;;Run the source
(run-until 200
           (at-beginning output-epsilon)
           (to-appended "ez"
             (at-every 0.4 E2)
             ))
;;after run meep:
;;h5topng -t 0:329 -R -Zc dkbluered -a yarg -A eps-000000.00.h5 ez.h5
```

Appendix B: Lorentz-Drude Model Constants for Ni, Ag, and Gold

Parameter	Ni	Ag	Au
ε	1	1	1
ω_p	15.92	9.01	9.03
ω_1	0	0	0
ω_2	0.174	.816	0.415
ω_3	0.582	4.481	0.83
ω_4	1.597	8.185	2.969
ω_5	6.089	9.083	4.304
ω_6	-----	20.29	13.32
Γ_0	0.048	0.048	0
Γ_1	4.511	3.886	0.415
Γ_2	1.334	0.452	0.83
Γ_3	2.178	0.065	2.969
Γ_4	6.292	0.916	4.304
Γ_5	------	2.419	13.32
f_0	0.096	0.845	0.76
f_1	0.1	0.065	0.024
f_2	0.135	0.124	0.01
f_3	0.106	0.011	0.071
f_4	0.729	0.84	0.601
f_5	------	5.646	4.384

References

[1] Homola, J.; Yee, S.S.; Gauglitz, G; Sensors and Actuators B 54 (1999) 3-15.

[2] Pitarke, J.M.; Silkin, V.M.; Chulkov, E.V.; Echenique, P.M.; *Rep. Prog. Phys.* **70** (2007) 1-87.

[3] Kik, P.G.; Brongersma, M.L.; *Surface Plasmon Nanophotonics*, Springer, The Netherlands (2007) pg. 1-2.

[4] Nylander, C.; Liedberg, B.; Lind, T.; *Sensors and Actuators*, **3** (1982/83) 79-88.

[5] Sun, Y.; Liu, X.; Song, D.; Tian, Y.; Bi, S.; Zhang, H.; *Sensors and Actuators B* **122** (2007) 469-474.

[6] Saj, W.M.; *Optics Express*, Vol **13** No 13 (2005).

[7] Fang, N.; Lee, H.; Sun, C.; Zhang, X.; Science 308 (2005) 534-537.

[8] Ferry, V.E.; Verschuuren, M.A.; Li, H.B.T.: Verhagen, E.; Walters, R.J.; Schropp, R.E.I.; Atwater, H.A.; Polman, A.; *Optics Express* Vol **18**, No 102 (2010).

[9] Holoma, J.; Piliarik, M.; *Surface Plasmon Resonance Based Sensors*, Springer, New York (2006) Pg 45.

[10] Jackson, J.D.; *Classical Electrodynamics*, 3rd ed. John Wiley & Sons, Inc. (1999) pg 237·

[11] Gaponenko, S.V.; *Introduction to Nanophotonics*, Cambridge Univ Press, New York (2010) pg 1.

[12] Rakić, A.D.; Djurišić, A.B.; Elanzar, J.M.; Majewski, M.L. *Applied Optics*. **37**,22 (1998)

[13] Stern E.A.; Ferrell, R.A. *Phys Rev*, **120**, 1 (1960).

[14] Sarid, D.; Challener W.; *Modern Introduction to Surface Plasmons*, Cambridge University Press, New York (2010) pg 201.

[15] Jain, P.K.; Lee, K.S.; El-Sayed, I.H.; El-Sayed, M.A.; J. Phys Chem B **11**, 7238-7248 (2006).

[16] Ye, D.; Mutisya, S; Bertino, M.; *Appl. Phys. Lett*. **99**, 081909 (2011).

[17] Kittel, C.; *Introduction to Solid State Physics*, 8th ed. John Whiley & Sons, Inc. (2005) pgs 187-219.

[18] Schock, H.W.; *Applied Surface Science* **92**, 606-616 (1996).

[19] Atwater, H.A.; Polman, A; *Nature Materials* **9**, 205-213 (2010).

[20] Pillai, S.; Catchpole, K.R.; Trupke, T.; Green, M.A.; *J Appl Phys* **101**, 093105 (2007).

[21] Kim, K.; Carroll, D.L. ; *Appl Phys Lett* **87**, 203113 (2005).

[22] Raman, C.V.; *Indian J Phys* **2** 387-398 (1928).

[23] Ferraro, J.R.; Nakamoto, K.; Brown, C.W.; *Introductory Raman Spectroscopy*, 2nd ed. (112-123) Academic Press, New York, 2003.

[24] Fleischmann, M.; Hendra, P.J.; McQuillan, A.J.; *Chem Phys Lett*. **26**, 2 (1974).

[25] Yee, K. E. *IEEE Transactions on Antennas and Propagation*, Vol. AP-14, No 3 (1966).

[26] Sullivan, D.M. *Electromagnetic Simulation Using the FDTD Method*. (1-2) *IEEE*, New York, 2000.

[27] Oskooi, A.F.; Roundy D.; Ibanescue, M.; Bermel, P.; Joannopoulos, J.D.; Johnson, S.G. *Computer Physics Communications* **181**, 687-702 (2010).

[28] http://ab-initio.mit.edu/wiki/index.php/Meep

[29] Mittra, R.; Pekel, Ü.; *IEEE Microwave and Guided Wave Letters* **5**, 3 (1995).

[30] Monk, P. *SIAM Journal on Numerical Analysis*, **29**, 3 (1992).

[31] Saleh B.E.A.; Teich, M.C.; *Fundamentals of Photonics*, 2nd Ed. John Wiley & Sons, Inc., Singapore (2007) pg 171.

[32] Saleh B.E.A.; Teich, M.C.; *Fundamentals of Photonics*, 2nd Ed. John Wiley & Sons, Inc., Singapore (2007) pgs 209-215.

[33] Jackson, J.D.; *Classical Electrodynamics*, 3rd ed. John Wiley & Sons, Inc. (1999) pgs 104-107.

[34] http://ab-initio.mit.edu/wiki/index.php/H5utils

[35] http://code.enthought.com/projects/mayavi/

[36] Sarid, D.; Challener W.; *Modern Introduction to Surface Plasmons*, Cambridge University Press, New York (2010) pg 206.

[37] http://www.mail-archive.com/meep-discuss@ab-initio.mit.edu/msg01270.html